Nature Communications

https://doi.org/10.1038/s41467-026-70000-6

Article in Press

Discovery of an ITK and TRK kinase inhibitor for the potential topical treatment of atopic dermatitis

Received: 24 September 2023

Accepted: 2 February 2026

Cite this article as: Duffen, J.L., Crouse, K.K., Ji, L. *et al.* Discovery of an ITK and TRK kinase inhibitor for the potential topical treatment of atopic dermatitis. *Nat Commun* (2026). https://doi.org/10.1038/s41467-026-70000-6

Jennifer L. Duffen, Kimberly K. Crouse, Lin Ji, Amy L. Brault, Kristen Ford, Jonathan Brooks, Scott A. Jelinsky, Yizheng Li, Julia H. Shin, Yajuan Zhao, Tatyana Andreyeva, Katherine Hammerman, Christina Arnold, Richard T. Sheldon, Jeonifer Garren, Wes LaBarge, Anthony Resek, Jon Volmer, Scott W. Bagley, Agustin Casimiro-Garcia, Gary M. Chinigo, Jennifer E. Davoren, Rajiah Aldrin Denny, Susan Drozda, Timothy L. Foley, Robert W. Hicklin, Shenping Liu, Frank E. Lovering, Nicole L. Nedoma, Mihir D. Parikh, Joseph W. Strohbach, John I. Trujillo, Stefanus J. Steyn, Karl Nocka, Martin Hegen, Fabien Vincent, Katherine L. Lee, Brian S. Gerstenberger & Michael J. Primiano

Discovery of an ITK and TRK Kinase Inhibitor for the Potential Topical Treatment of Atopic Dermatitis

Jennifer L. Duffen[1,#], Kimberly K. Crouse[1], Lin Ji[1], Amy L. Brault[1], Kristen Ford[1], Jonathan Brooks[1], Scott A. Jelinsky[1], Yizheng Li[1], Julia H. Shin[1], Yajuan Zhao[1], Tatyana Andreyeva[1], Katherine Hammerman[2], Christina Arnold[1], Richard T. Sheldon[1], Jeonifer Garren[3], Wes LaBarge[4], Anthony Resek[4], Jon Volmer[4], Scott W. Bagley[5], Agustin Casimiro-Garcia[6], Gary M. Chinigo[5], Jennifer E. Davoren[6], Rajiah Aldrin Denny[6], Susan Drozda[5], Timothy L. Foley[5], Robert W. Hicklin[5], Shenping Liu[5], Frank E. Lovering[6], Nicole L. Nedoma[5], Mihir D. Parikh[5], Joseph W. Strohbach[6], John I. Trujillo[5], Stefanus J. Steyn[7], Karl Nocka[1], Martin Hegen[1], Fabien Vincent[5], Katherine L. Lee[1], Brian S. Gerstenberger[6,#], & Michael J. Primiano[1,#]

[1]Inflammation and Immunology, Pfizer Inc, Cambridge, MA, USA; [2]Drug Safety Research and Development, Pfizer Inc, Cambridge, MA, USA; [3]Data Sciences and Analytics Pfizer Inc, Cambridge, MA, USA; [4]MedPharm Ltd, Durham, NC, USA; [5]Medicine Design, Pfizer Inc, Groton, CT, USA; [6]Medicine Design, Pfizer Inc, Cambridge, MA, USA; [7]Pharmacokinetics, Dynamics, and Metabolism, Pfizer Inc, Cambridge, MA, USA; [#]These authors jointly supervised this work.

Abstract

Interleukin-2-inducible T cell kinase is expressed by T cells and amplifies T cell receptor-dependent signals. Interleukin-2-inducible T cell kinase deletion or inhibition reduces production of interleukin-4 and interleukin-13, key drivers of atopic dermatitis. Nerve growth factor signals via the receptor tropomyosin-related kinase A and may promote pruritus in atopic dermatitis lesions. Here we describe PF-07245303, a compound which potently inhibits interleukin-2-inducible T cell kinase and

tropomyosin-related kinase family kinases capable of inhibiting T cell receptor-mediated cytokine production from CD4 and CD8 T cells and suppressing nerve growth factor-induced human basophil activation. In human skin explants, PF-07245303 demonstrates inhibition of tropomyosin-related kinase A phosphorylation, suppresses cytokine expression from T cell receptor-activated resident T cells and reverses the expression of atopic dermatitis associated genes. Topical application of PF-07245303 reduces proinflammatory and epidermal changes in a dermatitis model using female mice. By inhibiting both pathogenic inflammatory mechanisms, PF-07245303 may have therapeutic value for patients with atopic dermatitis.

Introduction

Atopic dermatitis (AD) is the most common chronic inflammatory skin disease with a 25% prevalence in children and a 7% prevalence in adults[1]. Atopic dermatitis patients suffer from dry and pruritic skin lesions which can affect their quality of life[2,3]. Genetic and environmental factors can contribute to skin barrier disruption and to immune hyper-activation, which are key drivers of atopic dermatitis pathogenesis[3]. T cell driven inflammation contributes to atopic dermatitis pathogenesis, and topical agents which can suppress the aberrant T cell activity may provide benefit to patients with this disease[1,4].

Interleukin-2-inducible T cell kinase (ITK) is a member of the Tec family of tyrosine kinases[5,6]. ITK expression is largely limited to immune cells such as T, NK, NKT, and mast cells[5,7]. In T cells, ITK amplifies T cell receptor (TCR)-dependent signals leading to cytokine production and cell proliferation[8–10]. Upon TCR activation, lymphocyte-specific protein tyrosine kinase (LCK) phosphorylates and activates ITK which in turn phosphorylates phospholipase C-γ1 (PLC-γ1)[10,11]. Activated PLC-γ1 generates second messengers diacylglycerol (DAG) and inositol 1,4,5-triphosphate (IP_3) via the hydrolysis of phosphatidylinositol 4,5-biphosphate (PIP_2), and these second messengers

activate protein kinase C theta (PKCθ) and calcium mobilization leading to activation of transcription factors NF-κB and NFAT and cytokine expression[11,12]. ITK is important for in vivo T cell responses, as ITK-deficient mice and/or mice treated with an ITK kinase inhibitor demonstrate reduced disease in models of type I diabetes, multiple sclerosis, lymphoproliferative disease, colitis, allergy/asthma, and airway hyperresponsiveness[9,13–18]. Transgenic mice expressing kinase-dead ITK are protected from OVA-induced pulmonary inflammation, supporting the role for ITK kinase activity in mediating Th2 inflammation[19]. Moreover, ITK-deficient mice or mice treated with a reported ITK kinase inhibitor demonstrate reduced skin inflammation in contact hypersensitivity-induced and imiquimod-induced models of dermatitis[20–22].

The pathogenic role for T cells and the Th2 cell-derived cytokines IL-4 and IL-13 in atopic dermatitis has been demonstrated through the clinical efficacy of dupilumab, an antibody to the IL-4 receptor that blocks the activity of both IL-4 and IL-13[1]. *ITK* deletion or inhibition of ITK kinase activity in T cells results in suppression of TCR-induced IL-4 and IL-13 production[1,15,23]. Elevated levels of *ITK* were described in peripheral T cells from patients with moderate to severe atopic dermatitis, and *ITK* expression is elevated in skin lesions from atopic dermatitis patients[20,24]. Additionally, Th1 cells, Th22 cells, and Th17 cells and the cytokines which they produce, IFNγ, IL-22, and IL-17, respectively, also contribute to atopic dermatitis pathogenesis[1,3,4]. The inactivation of ITK kinase activity has also been demonstrated to reduce Th1 and Th17 cell cytokine expression[25]. A therapeutic approach to inhibit the activation of these different T cell subtypes and to suppress the cytokines which they produce might provide efficacy beyond antagonism of only IL-4 and IL-13 signaling in atopic dermatitis patients.

Pruritus is a major factor contributing to reduced quality of life for atopic dermatitis patients[2,26]. Nerve growth factor (NGF) is a neurotrophic factor which regulates development, growth, and maintenance of neurons, and NGF can sensitize nociceptors and promote pruritus in the skin[27–29]. NGF signals via the receptor tropomyosin-related kinase A (TRKA), and both NGF and TRKA are present in skin[27,28].

Expression of NGF and TRKA is enhanced in atopic dermatitis skin lesions, and levels of NGF in skin lesions from atopic dermatitis patients correlate with itch severity[27,28,30–32]. TRKA and receptor kinases tropomyosin-related kinase B (TRKB) and tropomyosin-related kinase C (TRKC) are expressed by cells in the skin such as keratinocytes, neurons, mast cells, and basophils[28,33]. NGF induces keratinocyte proliferation, promotes basophil activation, stimulates mast cell degranulation, and contributes to neurogenic itch and inflammation[28,31,33,34]. A therapy which can suppress pruritus might provide symptomatic relief for patients with AD, and it may break the itch-scratch cycle which contributes to barrier disruption, further exacerbating the course and chronicity of the disease.

Here we describe PF-07245303, a dual inhibitor of ITK and TRK (TRKA, TRKB, and TRKC), kinases with potent activity in biochemical and cell-based assays. PF-07245303 was designed with properties suitable for topical formulation and delivery. This compound demonstrated potent inhibition of TRKA signaling, T cell activation, and cytokine expression in human skin explant models. A compound capable of inhibiting ITK kinase activity and TRK family kinase activity may have therapeutic value in atopic dermatitis and other numerous inflammatory, including allergic skin diseases, such as contact hypersensitivity, by suppressing dermal inflammation.

Results

Identification of PF-07245303, binding profile, and kinase selectivity

Efforts to discover ITK inhibitors have been described[35], including Pfizer's efforts to identify a potential allosteric inhibitor and an ATP competitive covalent inhibitor[36,37]. The discovery of PF-07245303 included use of structure-based drug design with parallel optimization for desired properties of a soft topical drug, including permeability and solubility to enable access skin tissue compartments and high metabolic clearance to reduce systemic exposure (Figure 1a). Literature examples[35,37] were screened in an ITK biochemical assay using 1 mM ATP, and the kinase hinge binding interaction was optimized to lead to the identification of a 2-(1H-pyrazol-5-yl)-1H-benzo[d]imidazole hinge binding moiety. This

moiety makes three-point hydrogen bond contacts with the carbonyl of Glu436 and the amide NH and carbonyl of Met438 (Figure 1b). The type 1 ATP competitive inhibitor makes extensive hydrophobic interactions with the ATP site of the kinase: for example, the cyclopropyl group makes contacts with side chains of Val377, Ala389, Lys391 and Phe435. Furthermore, the cyclopropyl moiety reduces planarity in the molecule (Figure 1b) and may contribute to selectivity against other kinases. Structure activity relationship studies identified the 5-methylhexahydrocyclopropane moiety, important for key lipophilic interactions with the p-loop region and improved potency and cellular permeability. Further modulation of physicochemical and ADME properties was achieved by incorporation of a 2-morpholinopyranmide, a weakly basic group with high sp^3 character to provide solubility in topical formulations. In addition to potent inhibition of ITK, crossover inhibition of TRKA, B and C kinases was discovered[38]. The identification of this selective polypharmacology, although not an initial objective, offered the potential value of additional efficacy and warranted further investigation.

The binding kinetics of PF-07245303 to its targets were determined by flowing compound dilutions over immobilized recombinant protein and measuring binding and dissociation. Kinetic rate constants (k_a and k_d), binding affinity (K_D), and $T_{1/2}$ were calculated. The affinity for PF-07245303 binding to ITK was 0.71 nM. Binding affinities to TRKA, TRKB, and TRKC were 2.94, 8.73, and 10.0 nM respectively (Figure 1c).

The physicochemical properties of PF-07245303 were tuned for the topical drug space[39] (Figure 1d). PF-07245303 demonstrates high permeability as judged by MDCK-LE cell line (13×10^{-6} cm/s) and moderate-to-high clearance in human hepatocyte incubation (30 µL/min/mil)[40]. The human clearance of PF-07245303 was predicted to be 11 mL/min/kg from scaled human hepatocytes using the parallel tube model. This predicted moderate-to-high human clearance is consistent with a soft drug approach in which the concentration of the drug is high at the site of action, i.e., skin, while the drug is rapidly

cleared from systemic circulation[41]. Additionally, crystalline PF-07245303 displays water solubility of 40.5 µM at pH 7.4.

To confirm that PF-07245303 is a potent and selective inhibitor of ITK and TRK family kinases, it was tested at 1 µM in a screening panel of 218 kinases (Figure 1e, Supplemental Table 1) at 1 mM ATP. PF-07245303 demonstrated the highest percent inhibition for kinases ITK (100%), TRKA (101%), TRKB (99%), and TRKC (97%) (Figure 1e). Follow up IC_{50} determinations were performed for kinases with inhibition greater than 50% of maximal response at 1 µM. All kinases identified except for Fms related receptor tyrosine kinase 3 (FLT3) (84%) showed greater than 38-fold selectivity compared to ITK. A follow-up cell-based NanoBRET system using HEK293 cells was used to determine cellular selectivity versus FLT3. Cellular activity in this assay showed ITK potency with an IC_{50} of 9.26 nM compared to IC_{50} of 1,130 nM (Supplemental Table 2) for FLT3 thereby supporting >100-fold selectivity of PF-07245303 for ITK vs FLT3 in a more physiologically relevant context. In addition, selectivity against related Tec family kinases BTK, TEC and LCK, which is a critical kinase for T cell receptor signaling, was evaluated. As shown in Supplemental Table 2, PF-07245303 demonstrated greater than 100-fold selectivity against these other kinases relative to ITK in the NanoBRET kinase cell-based assay.

PF-07245303 is a potent inhibitor of ITK kinase activity and inhibits ITK-dependent signaling and T cell activation

PF-07245303 demonstrated potent inhibition of ITK kinase activity in a biochemical assay using full-length human ITK protein. PF-07245303 inhibited ITK enzymatic activity in the presence of 1 mM ATP with an IC_{50} of 5.62 nM (Figure 2a). PLCγ1 is a substrate for ITK kinase, and PLCγ1 is phosphorylated in response to TCR-dependent signaling[6]. We assessed the cellular potency of PF-07245303 by measuring inhibition of ITK-mediated phosphorylation of PLCγ1 on residue Y783 in stimulated Jurkat T cells. Immunoblot analysis of lysates from Jurkat T cells stimulated with anti-CD3 and anti-CD28

antibodies in the presence of PF-07245303 demonstrated concentration-dependent inhibition of PLCγ1 phosphorylation with an IC_{50} of 154 nM (Figure 2b).

We next evaluated the ability of PF-07245303 to inhibit TCR-induced activation in isolated primary human T cells and T cells in human blood. As shown in Figure 2c, PF-07245303 demonstrated potent inhibition of anti-CD3 and anti-CD28 antibody-mediated stimulation of the T cell derived cytokine IL-2 from isolated human CD4+ T cells with an IC_{50} value of 38.5 nM. PF-07245303 was profiled for translation of potency in the highly proteinaceous human blood environment by measuring inhibition of IL-2 production from human blood T cells stimulated in vitro with anti-CD3, anti-CD28 and anti-CD2 antibodies. PF-07245303 inhibited the release of IL-2 in blood with an IC_{50} value of 1350 nM (Figure 2d). PF-07245303 was determined to be moderately bound to human plasma protein with mean fraction unbound values of 0.144 as determined by equilibrium dialysis at 2 μM with blood to plasma ratio of 1.60[42,43]. Correcting this whole blood IC_{50} value for unbound intrinsic compound results in a potency of 122 nM. To rule out the possibility that the TRK kinase inhibition is responsible for the cytokine inhibition, we tested a compound, PF-06273340[44], which selectively inhibits TRK kinases, in the human T cell and whole blood assays. As shown in Supplemental Figure 1, PF-06273340 did not inhibit ITK kinase activity and did not suppress TCR-induced T cell IL-2 production. Thus, PF-07245303 is a potent inhibitor of ITK kinase activity and suppresses T cell activation as demonstrated by inhibition of TCR-induced, ITK-dependent PLCγ1 phosphorylation and suppression of IL-2 production from activated human T cells in vitro.

PF-07245303 inhibits cytokine production from CD4+ T cells, Th1, Th2, and Th17 differentiated cells, and CD8+ T cells

Activated T cells can secrete multiple cytokines which contribute to the pathogenesis of inflammatory diseases including atopic dermatitis[1]. Therefore, we evaluated the ability of PF-07245303 to suppress

the anti-CD3 and anti-CD28 antibody-induced cytokine production from primary human CD4+ T cells. In this assay system, PF-07245303 inhibited the release of pro-inflammatory cytokines IL-4, IL-13, IFNγ, IL-17A, and the anti-inflammatory cytokine IL-10 (Figure 3a – e), with IC_{50} values of 73.5 nM, 348 nM, 73.2 nM, 282 nM, and 114.5 nM respectively. TRK family selective compound PF-06273340 did not inhibit T cell production of IL-4, IL-13, IL-17A, nor IFNγ indicating that inhibition of TCR activation-induced cytokines by PF-07245303 is dependent on ITK kinase inhibition (Supplemental Figure 2a-d).

Th1, Th2, and Th17 are subsets of effector CD4+ T cells which produce an array of cytokines which contribute to inflammatory and autoimmune disease[5,12]. Therefore, we sought to evaluate the impact of ITK kinase inhibition with PF-07245303 on the differentiation of naïve CD4+ T cells to Th1, Th2 and Th17 cells subsets and subsequent cytokine production. In a dose-dependent manner, PF-07245303 inhibited the release of IFNγ, IL-13 and IL-17A from stimulated human naïve CD4+ T cells skewed to Th1, Th2 and Th17 (Figure 3f – h), respectively, with IC_{50} values of 35.4 nM for IFNγ release, 60.9 nM for IL-13 release, and 12.5 nM for IL-17A release. In summary, PF-07245303 inhibited the production of pro-inflammatory cytokines IFNγ, IL-13, and IL-17A which can drive inflammatory diseases including vitiligo[45], atopic dermatitis[1], and psoriasis[4], respectively. Moreover, CD8+ T cells and IFNγ can contribute to skin conditions such as vitiligo[45] and alopecia areata[46]. Therefore, we demonstrated that PF-07245303 was also capable of potently inhibiting IFNγ release from TCR-activated human CD8+ T cells with an IC_{50} of 18.9 nM (Supplemental Figure 2e).

PF-07245303 is a potent inhibitor of tropomyosin-related kinase receptor TRKA, TRKB, and TRKC kinase activity

Pruritus associated with atopic dermatitis can reduce patient quality of life and contribute to barrier disruption which amplifies disease[3,26]. As NGF can sensitize nociceptors and promote pruritus in the

skin[27–29], inhibition of the receptor kinase TRKA which transmits NGF signals may reduce itch and benefit patients with AD. In addition to its ability to inhibit ITK kinase activity, PF-07245303 is a potent inhibitor of tropomyosin-related kinase receptors TRKA, TRKB, and TRKC activity in biochemical assays. Using the cytoplasmic domains of human TRKA, TRKB, and TRKC, PF-07245303 inhibited the kinase activity of these enzymes in the presence of 1 mM ATP with mean IC_{50} values of 7.2 nM, 12.0 nM, and 20.7 nM, respectively (Figure 4a – c).

The cell-based potency of PF-07245303 was determined at DiscoverX using their PathHunter® system which uses an enzyme functional complementation technology. This assay was used to assess the inhibitory effects of PF-07245303 and the highly potent and selective pan-TRK inhibitor PF-06273340 on TRKA-, TRKB- or TRKC-dependent phosphorylation. Cells utilized in the assay were U2OS cells which expressed human TRKA, TRKB or TRKC and the low affinity pan-neurotrophin receptor p75 (Figure 4d – f). PF-07245303 demonstrated inhibition of TRKA-, TRKB- or TRKC-dependent phosphorylation in the presence of p75 with IC_{50} values of 72.6 nM, 48.7 nM, and 21.7 nM respectively. Similar potencies were observed in the same assay system when the cells expressed TRKA, TRKB, or TRKC in the absence of p75 (Supplemental Figure 3a – c). Furthermore, we sought to evaluate the activity of this compound in primary human cells with endogenous expression of TRKA. To that end we measured the ability of PF-07245303 to suppress NGF-induced activation of human basophils which express TRKA mRNA and protein and are associated with inflammatory skin diseases[47,48]. PF-07245303 and the selective pan-TRK inhibitor PF-06273340 demonstrated inhibition of NGF-dependent increases in the percent of human blood cells positive for CD203c, a marker of basophil activation and degranulation[47,49,50] with IC_{50} values of 442 nM and 109 nM, respectively (Figure 4g). Correcting for protein binding yields intrinsic compound potencies of 39.8 nM and 16.3 nM in this assay. We also evaluated the potential role for ITK in IgE receptor-dependent signaling in human basophils. PF-07245303, which does not inhibit BTK in the conditions tested, is effective at reducing IgE receptor-

mediated activation of primary human basophils, as measured by IL-4 release (Supplemental Figure 4). Collectively, these data demonstrate that PF-07245303 is also a potent inhibitor of TRKA, TRKB, and TRKC receptor kinases.

Measurement of NGF-induced TRKA phosphorylation in ex vivo human skin tissue and effect with PF-07245303 treatment

As inhibition of ITK and TRK kinase activity might provide utility in the treatment of inflammatory skin diseases, we sought to demonstrate pharmacological activity of PF-07245303 in an ex vivo human skin model. NGF selectively binds to TRKA inducing receptor dimerization and TRKA autophosphorylation[51]. Quantification of the reduction in NGF-induced TRKA phosphorylation provides a proximal measure of TRKA kinase inhibition and target engagement. To this end, we established a previously described experimental system to measure TRKA phosphorylation and target engagement in human skin explants when the skin tissue is treated with NGF[52]. We also employed our observations that Th2 cytokines can enhance *TRKA* expression by pre-treating the skin sections with IL-4 and IL-13 for 24 hours before stimulating the ex vivo skin with NGF. This experimental system allowed for the measurement of compound-dependent inhibition of TRKA phosphorylation in human skin tissue treated with PF-07245303.

Following pretreatment with IL-4 and IL-13, human ex vivo skin sections were treated with NGF for 5 minutes and TRKA detected in skin protein lysates by an ELISA method to capture human TRKA followed by detection of phosphorylated TRKA using a phospho-TRKA antibody. As shown in Figure 4h, we observed an enhancement in levels of phospho-TRKA in skin sections pretreated with Th2 cytokines and stimulated with NGF relative to untreated or only Th2 cytokine treated skin. In skin sections treated with PF-07245303 (10 μM to 0.1 μM) at the time of NGF treatment, we observed concentration-dependent inhibition with almost complete inhibition of phospho-TRKA levels with 10,

3, and 1 µM compound (Figure 4h, Supplemental Table 3). Similarly, 10 µM of the potent and selective pan-TRK inhibitor PF-06273340 decreased TRKA phosphorylation. These results demonstrate that PF-07245303 inhibits activation of TRKA in human skin tissue indicating that adequate concentrations of PF-07245303 were achieved to engage the TRKA target and to demonstrate pharmacology.

PF-07245303 inhibits activation of resident dermal T cells in ex vivo human skin sections stimulated with anti-CD3 and anti-CD28 antibodies

We showed that PF-07245303 could inhibit activation of TRKA kinase in NGF-treated ex vivo human skin. Infiltration of T cells and production of T cell-derived cytokines can contribute to atopic dermatitis, psoriasis, and other dermatological diseases[4]. Therefore, we sought to evaluate the capability of the ITK and pan-TRK kinase inhibitor PF-07245303 to suppress activation of skin-resident T cells and reduce the production of pro-inflammatory cytokines. Treatment of human ex vivo skin sections with anti-CD3 and anti-CD28 antibodies activates skin-resident T cells and induces expression of pro-inflammatory cytokines[53]. As shown in Figure 5a – c, we demonstrated that anti-CD3 and anti-CD28 antibodies induce expression of *IFNG*, *IL13*, and *IL2* in stimulated ex vivo human skin tissue and enhance production of IL-2 protein detected in the skin culture media relative to unstimulated skin (Figure 5d). With simultaneous addition of 10 or 3 µM PF-07245303 with T cell activating antibodies to the skin culture media, we observe concentration-dependent and almost complete inhibition of anti-CD3 and anti-CD28-induced *IFNG*, *IL13*, and *IL2* gene expression (Figure 5a – c and Supplemental Table 4). Likewise, PF-07245303 treatment of ex vivo human skin almost completely suppressed the quantity of IL-2 protein detected in the skin culture media at compound concentrations of 10, 3, and 1 µM (Figure 5d, Supplemental Table 5). Similar to data from Smith et al.[53], these results indicate that skin-resident T cells can be activated in human skin explants. Furthermore, with addition of PF-07245303 to the culture media exposed to the basolateral side of the skin, adequate concentrations of inhibitor were achieved in

skin tissue to attenuate TCR-dependent activation of cytokine expression. To further evaluate the effects of ITK and TRK inhibition in a more physiological model, PF-07245303 was formulated in a fit-for-purpose[54] vehicle (0.2% or 1.0%) and applied to the apical side of ex vivo human skin. Topically administered PF-07245303 significantly reduced Th2 cytokine and TCR-stimulated *IFNG*, *IL13*, *IL2* and *IL17A* gene expression by 72.8 – 88.0% relative to vehicle control (Figure 6a-d, Supplemental Table 6). These data suggest that in human skin tissue the ITK and pan-TRK kinase inhibitor PF-07245303 can reduce T cell activation-dependent expression of pro-inflammatory cytokines which are known to contribute to the inflammation and pathogenesis of atopic dermatitis and other dermatological diseases.

In the human skin explant model PF-07245303 reverses the expression of many genes associated with atopic dermatitis

We created a disease gene expression signature from human skin explant cultures. Cultures were stimulated with anti-CD3/anti-CD28 and a Th2 cytokine cocktail to mimic the Th2 response seen in atopic dermatitis lesional samples. Anti-CD3/anti-CD28 stimulations with Th2 cytokines regulated the expression of 6128 genes (FDR <0.05) (Figure 7a). Using publicly available RNA sequencing data from atopic dermatitis patient lesional skin[55], we show that most genes regulated by anti-CD3/anti-CD28 are also regulated in the same direction in disease tissue (Figure 7b). We also determined the expression profile of skin explant cultures treated with PF-07245303 and show that the majority of genes induced by anti-CD3/anti-CD28 stimulation are reversed by treatment with PF-07245303 (Figure 7c). PF-07245303 treatment reversed anti-CD3/anti-CD28 induced expression of many immune related genes, including *CXCL11*, *IFNG*, *IL2*, *IL4*, *IL13*, *IL17A*, *FLG*, *FLG2*, *IL31RA*, *NGF*, *OSMR* and *IL4R*. (Figure 7d).

PF-07245303 treatment reduces ear thickness, ear tissue cytokines, and disease severity in a mouse model of oxazolone-induced dermatitis

Having demonstrated that both basolateral and topical application of PF-07245303 in human skin explants can inhibit anti-CD3 and anti-CD28-induced activation of resident dermal T cells, we employed the oxazolone-induced contact hypersensitivity mouse model of dermatitis to evaluate the ability for PF-07245303 to reduce skin inflammatory responses in vivo. It is worth noting that the oxazazolone-induced model of dermatitis does not fully mimic the complex features of clinical AD[56] . With oxazolone challenge, increased ear thickness was observed in the vehicle group while 43% - 61% inhibition of ear thickness was observed with topically applied 2% PF-07245303 at days 4, 7, 9, and 11 after initiation of oxazolone challenge (Fig. 8a, supplemental table 7). In ear skin sections, typical mixed inflammatory cell infiltration into the dermis and epidermal changes (hyperplasia, ulceration/erosion/thinning, superficial hyperkeratosis/crusting) were observed with oxazolone challenge. Visual and histological composite disease scores were moderately lower in oxazolone-challenged mice treated with PF-07245303 (Fig. 8 b-f, supplemental table 8). Protein levels for IL-4, IL-10, IL-17A, GM-CSF, and TNFα, were moderately decreased while levels of IL-2 and IFNγ were not different with PF-07245303 treatment (Fig. 8 g-j, supplemental Fig. 5, and supplemental table 9). Histological evaluation of PF-07245303 effects on dermal inflammatory cell infiltrates and changes in epithelial endpoints such as hyperplasia, ulceration, thinning, and surface hyperkeratosis shows moderate decrease in disease scores (supplemental Fig. 5). Collectively, these results suggest that application of PF-07245303 can reduce proinflammatory and epidermal barrier changes associated with atopic dermatitis.

Discussion

Herein, we describe the in vitro pharmacology of PF-07245303, a dual ITK and TRK family kinase inhibitor designed with physiochemical properties associated with successful topical agents[39]. ITK is an important component of TCR-dependent T cell activation and PF-07245303 demonstrated potent in vitro inhibition of the production of Th2 cytokines IL-4 and IL-13 known to drive atopic dermatitis[5,12,57]. Additionally, PF-07245303 potently inhibits TCR-induced production of Th1 and Th17 cytokines which can contribute to AD pathogenesis and other inflammatory skin diseases[1,4,58,59]. PF-07245303 also demonstrates potent inhibition of TRKA, TRKB, and TRKC kinase activity in biochemical assays and recombinant cell systems. NGF levels and levels of its signaling receptor, TRKA, are increased in skin of patients with atopic dermatitis and correlated with pruritus severity[30,31]. Moreover, we demonstrate dual ITK and TRKA-dependent pharmacology of PF-07245303 in ex vivo human skin sections as well as the ability of this compound to suppress expression of pro-inflammatory genes known to contribute to dermatitis and to reverse the AD-associated gene signature observed in patient lesions.

Due to the key role for ITK in many different models of inflammatory diseases[5,60], there have been numerous efforts to design and develop selective ITK kinase inhibitors including allosteric inhibitors, covalent inhibitors, and ITK degrader compounds[36,37,61–66]. Studies of ITK-deficient mice suggest that ITK may play a significant role in development of Th2 responses and allergic asthma[13,15,67]. Further, the important role for the kinase activity of ITK was demonstrated by reduced OVA-induced airway hyper-reactivity in ITK kinase dead transgenic mice[19]. Surprisingly, treatment of mice with an ITK kinase inhibitor did not reduce OVA-induced Th2 response nor airway hyper-responsiveness; increased Th2 cytokines and T cell hyperplasia were observed[23]. Using a different ITK inhibitor, Nadeem et al. observed reduced LPS-induced airway inflammation in a mouse model of acute lung injury[22]. PF-07245303 demonstrated potent in vitro inhibition of TCR-induced Th2 cytokines IL-4 and IL-13

production from primary human T cells and may provide benefit in Th2 driven diseases such as atopic dermatitis.

There is an increasing appreciation for the role of ITK in promoting Th1 and Th17 cell responses, as ITK deletion or inhibition of ITK kinase activity has been found to reduce the TCR-dependent production of numerous pro-inflammatory cytokines such as IL-2, IL-9, IL-17, and IFNγ from T cells in vitro [18,25,68,69]. Similarly, inhibition of ITK kinase in isolated primary human T cells with PF-07245303 resulted in potent inhibition of Th2 cytokines IL-4 and IL-13 as well as Th1 and Th17 cytokines IFNγ and IL-17A respectively. Moreover, ITK kinase inactivation with small molecule inhibitors has been demonstrated to reduce the levels of the pro-inflammatory cytokines IL-2, IL-4, IL-17, IL-22, IFNγ, and TNF-α in tissues from mouse models of dermal inflammation[20–22]. Subcutaneous delivery of a small molecule ITK inhibitor reduced dermal inflammation and ear swelling in mouse models of contact hypersensitivity, and decreased levels of IL-2, IL-4, or IFNγ expression were observed in ear tissue samples from the model(s)[20]. In two different studies, topical administration of an ITK kinase inhibitor reduced ear swelling and dermal inflammation in the imiquimod-induced skin inflammation model which was associated with reduced expression of pro-inflammatory cytokines and a reduction of Th17 cells in the skin[21,22]. These results and our demonstration that inhibition of ITK kinase in isolated primary human T cells with PF-07245303 resulted in potent inhibition of Th2 cytokines as well as Th1 and Th17 cytokines, IFNγ and IL-17A, and reduced disease severity in a mouse dermatitis model suggest that ITK and TRK kinase inhibition may prove efficacious in many inflammatory dermatological diseases including atopic dermatitis, psoriasis, and vitiligo.

To translate effects of ITK inhibition to human tissue, we used a skin explant model to investigate the ability for PF-07245303 to inhibit expression of proinflammatory cytokines from resident T cells in human skin[53,70]. We observed enhanced expression of *IL2*, *IL13*, and *IFNG* when human skin is treated ex vivo with anti-CD3 and anti-CD28 antibodies to stimulate resident T cells. Importantly, treatment of

the skin explant with PF-07245303 demonstrated moderate to high inhibition of *IL2*, *IL13*, and *IFNG* expression in a concentration-dependent manner. This data demonstrates proof of pharmacology for our ITK kinase inhibitor in the relevant human tissue.

Itch is a frequent symptom of atopic dermatitis which can dramatically affect quality of life for patients with this disease[2,26]. NGF levels and levels of its signaling receptor, TRKA, are increased in the skin of patients with atopic dermatitis and correlate with pruritus severity. NGF has been demonstrated to contribute to pruritus and inhibition of TRKA has been shown to reduce scratching in the NC/Nga mouse atopic dermatitis model[71]. In a clinical trial in psoriasis patients, topical treatment with a reported TRKA kinase inhibitor resulted in significant attenuation of pruritus[72]. Additionally, BenevolentAI advanced a topical pan-TRK inhibitor BEN-2293 (1%) into clinical study (NCT04737304) with mild-to-moderate atopic dermatitis patients[73] . As a potent inhibitor of TRKA kinase activity, PF-07245303 treatment of basophils in human blood could inhibit NGF-dependent basophil activation as measured by CD203c levels[47,49,50]. Basophils are present in skin of patients with pruritic diseases such as atopic dermatitis, prurigo, urticaria and increased levels of CD203c on basophils have been described in the blood of patients with these diseases[47]. Moreover, basophils have been demonstrated to be necessary for itch flares in a mouse model of atopic dermatitis-associated inflammation[47,74]. Additionally, NGF treatment of human basophils primes these cells to release inflammatory mediators, and NGF induces production of the cytokine mediator of atopic dermatitis IL-13[75]. IL-4 and IL-13 may also contribute to pruritus as patients with atopic dermatitis treated with dupilumab experienced significant reductions in itch[76].

Alterations of numerous genes have been described in lesions from atopic dermatitis patients[1,55]. Many pro-inflammatory genes are upregulated with disease, and many genes whose products are important for skin barrier formation such as filaggrin are decreased with disease[1,57]. We used the human skin explant model in which human skin sections were treated ex vivo with anti-CD3 and anti-CD28 antibodies and a

Th2 cytokine cocktail to mimic atopic dermatitis lesions. In this model, we evaluated the effects of treatment with PF-07245303 by bulk RNAseq to evaluate relevant gene expression. When comparing the anti-CD3 and anti-CD28 and Th2 cytokine stimulated skin in the absence of compound with the gene expression profile observed in skin lesions from atopic dermatitis patients, we observed a remarkable similarity in differentially expressed genes (DEGs) suggesting that this skin explant model can mimic many of the transcriptional changes observed in patient skin. Strikingly, when stimulated skin sections were treated with PF-07245303 we observed a significant reduction in many genes upregulated in the model and upregulated in AD lesions such as pro-inflammatory cytokines. Moreover, we observed a reversal in the decreased expression of genes associated with barrier protection in our model.

The dual ITK and TRK family kinase inhibitor PF-07245303 demonstrated disease relevant pharmacology in cellular systems, in a mouse model of dermatitis, and in human skin ex vivo. By inhibiting the kinase activity of ITK, which amplifies TCR signaling in T cells, with PF-07245303 we aspire to have a therapeutic agent capable of suppressing T cell-dependent inflammation and cytokine production driving atopic dermatitis. Additionally, by also inhibiting TRK family kinase activity we postulate this agent may coincidently reduce the discomfort of AD-associated itch and break the itch-scratch cycle which can amplify the disease. Thus, topical application of PF-07245303 aims to reduce dermal inflammation and disease severity while also providing patients with relief from pruritus associated with atopic dermatitis and other skin diseases.

Methods

Ethics Statements

Primary human blood samples were obtained with informed written consent from healthy human adult donors in accordance with the Pfizer Inc. Global Colleague Wellness Research Support Program

(protocol CW RDP-02, IRB number: 08-33390) approved by the Advarra Institutional Review Board. Human skin tissue was obtained via elective abdominoplasty with written donor consent under Pearl IRB approval in accordance with FDA 21 CFR 56.104 and DHHS 45 CFR 46.101 regulations (Pearl Pathways. Exemption Determination Submission. IRB Study Number: 15-MEDP-101. All procedures performed on animals were in accordance with regulations and established guidelines and were reviewed and approved by a Pfizer's Institutional Animal Care and Use Committee or through an ethical review process. Pfizer animal care facilities that supported this work are fully accredited by AAALAC International and abide by ARRIVE guidelines.

Crystallography

Crystallization of ITK has been reported previously[37] . Crystals of ITK-KD (ITK kinase domain) were grown by the hanging-drop vapour diffusion method at room temperature (22°C). Purified ITK at 3 mg/ml was incubated with 0.5-1 mM inhibitor for approximately 30 minutes prior to crystallization trials. Crystallization drops were set up with 1 µl of protein plus 2 µl of reservoir containing approximately 12% PEG 3350, 0.1 M magnesium acetate and 0.1 M HEPES, pH 7.2. Crystals grew overnight and were flash frozen in liquid nitrogen after transfer to a cryoprotectant solution containing mother liquor plus 20%(v/v) glycerol. Crystal structure data collection and refinement statistics can be found in supplemental section.

Kinase Selectivity Assays

PF-07245303 was evaluated at Carna Biosciences, Inc. (Kobe, Japan) using off-chip mobility shift assays run in duplicate using 218 kinases. Details of kinase assay method available in supplemental methods section.

Measurement of Binding Kinetics using SPR

A CM5 sensor chip was loaded into the T200 Biosensor (Cytiva) and primed with HBS-EP (10 mM HEPES pH 7.4, 150 mM NaCl, 3 mM EDTA, 0.005% tween-20) buffer. Anti-His antibody (Genscript, Piscataway, NJ) was immobilized onto flowcells 1 and 2 using standard amine coupling conditions resulting in 8-10K RU of immobilized antibody. Recombinant His-tagged human ITK (Lake Pharma, Belmont, CA) was diluted into HBS-EP and injected over a single anti-His flowcell for 30 minutes at 5 µl/min flowrate. The captured ITK was then cross-linked with a 30s injection of 1:1 pre-mixed NHS/EDC, followed by 30s of ethanolamine (amine coupling kit, Cytiva) resulting in a level of captured and cross-linked ITK protein ranging from 7K – 10K RU. Biotinylated human TRKA, TRKB, and TRKC proteins (Carna Biosciences) were immobilized onto individual flowcells of a Streptavidin (SA) sensor chip using standard immobilization conditions resulting in 4K-10K RU of immobilized TRKA, TRKB, and TRKC proteins. The following was performed on separate sensor chips containing either ITK or TRK proteins. Using the single-cycle kinetics method, compound was tested for binding in a 3-fold serial dilution of five concentrations ranging from 0.49 to 40nM passed over the ligand and reference channel. The association time was 60 seconds, and the dissociation time was 180 seconds for ITK and 60 – 480 seconds for TRKA, TRKB and TRKC at a flowrate of 50 µl/minute for all proteins tested. Buffer injections and DMSO calibration curve were included for referencing the data. Data analysis was performed using Biacore T200 evaluation software version 3.2.2. The double-referenced and solvent corrected data were fit to a 1:1 binding model to calculate rate parameters and affinity constant. $T_{1/2}$ was calculated using the following equation: $T_{1/2}$ = (nl2 / kd)/60 where nl (natural log) of 2 (0.693) is divided by the kd, to calculate $T_{1/2}$ in seconds. This value was then divided by 60 to present the value in minutes.

ITK Isolated Enzyme Potency

The effect of compound on ITK kinase activity was determined by measuring the inhibition of ITK kinase-dependent phosphorylation of a biotin-tagged BTK peptide (CPC # 923799, sequence Biotin-KKVVALYDYMPMN-NH2) as substrate in the presence of ATP detected with time-resolved fluorescence resonance energy transfer (TR-FRET). An 11-point dilution series of compound was prepared to yield final assay concentrations of compound of 30 µM down to 0.0003 µM in 1% DMSO. In 384-well plates, 7.5 µl of assay mixture containing recombinant full-length human ITK protein was added to wells containing 0.1 µL serially diluted compound and the assay plates were incubated for 30 minutes at room temperature. Next, 2.5 µL substrate solution containing ATP (Teknova, A1204) and biotin-BTK peptide (China Peptide Company, CPC # 923799) was added to the wells containing ITK enzyme and compound. The final kinase assay reaction mixture contained 0.25 nM ITK, 1 µM biotin-BTK peptide, 1 mM ATP, 20 mM HEPES pH 7.5, 0.01% gelatin, 10 mM $MgCL_2$, 5 mM GSH, and 0.01% Brij-35. Assay plates were incubated for 60 minutes at room temperature before adding to each well 10 µL of Stop/Detect Buffer (1 nM anti-phospho-tyrosine antibody labeled with Europium (LANCE PT66, Perkin Elmer, AD0069), 16.5 µg/ml Surelight streptavidin APC (Perkin Elmer, CR-130), HEPES pH 7.5, 0.01% gelatin, 10 mM EDTA, 250 mM NaCl) The plate was covered and allowed to incubate overnight at room temperature. Fluorescence was read with an EnVision plate reader with an excitation wavelength of 665 nm and an emission wavelength of 615 nm. The concentrations and resulting effect values for the tested compound were plotted and the concentration of compound required for 50% effect (IC_{50}) was determined with the four-parameter logistic dose response equation. The IC_{50} reported is the geometric mean of the IC_{50} determined for each individual experiment.

Inhibition of ITK-dependent Proximal Signaling in Jurkat T Cells

Jurkat T cells (Clone E6-1 from ATCC Cat# TIB152) were resuspended into cell media containing RPMI-1640, 10% Heat-inactivated FBS, 100 unit/mL Penicillin-Streptomycin, 2 mM L-glutamine, 10

mM HEPES, 1 mM Sodium pyruvate, MEM non-essential amino acids solution and 5 x 10^5 cells per well were plated into 12-well plates. Half-log serial dilutions of compound were prepared and added to the cells to yield final assay concentrations of 10 µM down to 0.0003 µM with 0.03% DMSO. Cells were treated with compound for 30 minutes at 37°C followed by activation with ImmunoCult human anti-CD3/CD28 T cell activator (StemCell Tech. 10971) at a 1:100 dilution for 5 minutes at 37°C. Cell pellets were lysed on ice for 30 minutes in Complete Tris lysis buffer containing a 1:100 dilution of protease/phosphatase inhibitor cocktail solution, and 1 mM PMSF. Whole cell lysates were disrupted in SDS-PAGE sample buffer, boiled at 90°C for 5 minutes and loaded on 4-12% polyacrylamide mini-gels. Soluble lysates were resolved by SDS-PAGE and transferred to nitrocellulose membranes using the iBlot 2 semi-dry gel transfer system. Membranes were blocked neat with a TBS-based blocking buffer for 1 hour at room temperature and probed overnight at 4°C with specific antibodies to PLCγ1 (1:1,000 dilution, MilliporeSigma 05-366), phospho-PLCγ1 Y783 (1:1,000 dilution, Cell Signaling Tech. 2821L) and β-actin (1:10,000 dilution, Cell Signaling Tech. 4967L). The membranes were washed with TBS with Tween-20 and incubated for 1 hour with IRDye secondary antibodies in TBS with Tween-20. Proteins were detected via infrared fluorescence using the Li-COR Odyssey CLx imaging system. Quantification of total and phosphorylated PLCγ1 protein was performed via densitometry analysis using Image Studio analysis software. Fold change was determined based on the phospho-PLCγ1 to total PLCγ1 signal ratio. Results from four independent analyses were then plotted against each compound concentration and used a three-parameter least squares fit regression model in GraphPad Prism Version 10.4.1 to determine IC_{50}.

Compound Potency in Primary Human T Cells

Human CD4+ T cells were isolated, activated with anti-CD3/CD28 for 3 days, and expanded for an additional 4-6 days as follows. Isolated human CD4 T cells were purchased from StemCell

Technologies (Cat. 70026) On day 0, CD4+ T cells were thawed, resuspended in assay medium (50% DMEM/50% RPMI with glutamine, 10% heat-inactivated human serum, 1x non-essential amino acids, 2 mM glutamine, and 1x penicillin/streptomycin), treated with anti-CD3/CD28 Dynabeads™ (ThermoFisher, 11161D), and incubated at 37°C/5% CO_2. On day 3, the beads were removed, and the cells diluted to $5x10^5$ cells/cm^2 and placed in G-Rex10™ flasks for incubation at 37°C/5% CO_2. The expanded CD4+ T-cells were centrifuged and resuspended to 0.5 million cells per ml and 60 µl of CD4+ T cells added per well (30,000 cells/well) to a 384 well plate containing 0.1 µL of an 11-point half log dilution series of compound in 100% DMSO. The final assay compound concentration range was 10 µM to 0.01 nM and 0.13% DMSO. The plates were incubated 15 min at 37°C/5% CO_2. Twenty µl of diluted ImmunoCult™ human anti-CD3/CD28 T Cell Activator (StemCell Technologies, 10991, 1:12.5 in T cell assay media) was added to all wells of the plate (1:50 final assay concentration). The plates were incubated an additional 20 to 24 hrs at 37°C/5% CO_2. The plates were centrifuged and 16 µL of supernatant was removed and combined with 4 µl of IL-2 HTRF antibodies (Cisbio kit, 62HIL02PEH). Plates were incubated for 3 hours at room temperature and read with EnVision™ plate reader at 665 nm and 615 nm wavelengths. Using the fluorescence intensity 665/615 ratio data the percent inhibition of each compound dose was evaluated. An unconstrained sigmoid curve was fitted using a 4-parameter logistic equation and an IC_{50} reported as the midpoint of the curve. The IC_{50} reported is the geometric mean of the IC_{50} values determined for each individual experiment.

Compound Potency in Human Whole Blood

Human peripheral blood was collected from donors in the Pfizer Research Support program via venous collection. Sixty µl per well of heparinized human whole blood was added to 384-well, polypropylene plates containing 0.08 µl of an 11-point half log dilution series of compound in 100% DMSO. The final assay compound concentration range was 30 µM to 0.3 nM in 0.1% DMSO. The plates were incubated

45 min at 37°C/5% CO_2. Twenty µl of diluted ImmunoCult Plus™ (StemCell Technologies, 1:25 in PBS/Glucose Buffer) was added to all wells (1:100 final assay concentration). The plates were incubated 20 to 24 hrs at 37°C/5% CO_2. The plates were centrifuged and 16 µL of plasma was removed and combined with 4 µl of IL-2 HTRF antibodies (Cisbio kit, 62HIL02PEH). Plates were incubated for 3 hours at room temperature and read with EnVision™ plate reader at 665 nm and 615 nm wavelengths. Using fluorescence intensity 665/615 ratio data the percent inhibition of each compound dose was calculated. An unconstrained sigmoid curve was fitted using a 4-parameter logistic equation and the IC_{50} was reported as the midpoint of the curve. The IC_{50} reported is the geometric mean of the IC_{50} values determined for each individual experiment. Partitioning of PF-07245303 between red blood cells and plasma at a concentration of 1 µM (n=4) and fraction unbound at a concentration of 2 mM in human plasma was measured in vitro by equilibrium dialysis (n=4) at York Bioanalytical Solutions, Sandwich UK.

T cell, Th1, Th2, and Th17 cytokine release assays

PBMCs were isolated from either a leukopak (StemCell Technologies or Research Blood Components) or from whole blood obtained with informed written consent from healthy human adult donors using Lymphoprep (StemCell Technologies). Naïve CD4+ T cells were isolated using the EasySep Human Naïve CD4+ T Cell Isolation Kit, according to manufacturer's instructions (StemCell Technologies). CD4+ T cells (StemCell Technologies) were thawed and allowed to rest in X-Vivo 15 + 1% penicillin/streptomycin at approximately $1x10^6$ cells/ml for 2 hours in an incubator at 37°C/5% CO_2. After two hours the cells were seeded into a 96-well plate at $0.1x10^6$ cells/well in 160µl/well of X-Vivo 15 + 1% Penicillin/streptomycin ($0.625x10^6$ cells/ml). Compounds were prepared at 10X and 20µl was added to appropriate wells (0.3% DMSO final) and incubated for 15 minutes at 37°C/5% CO_2. CD3/CD28 T cell activator Dynabeads were washed in media and then added at 1 bead/cell (20µl of

beads/well at $5x10^6$ beads/ml) to appropriate wells. Cells were incubated overnight (20 to 24 hours) at 37°C/ 5% CO_2. The next day supernatants were harvested and frozen at -80ºC for later analysis. Cytokine content was measured using Meso Scale Diagnostics (MSD, Rockville, MD, USA) Proinflammatory Panel 1 (C-0049-2) and Cytokine Panel 1 (C-0050-2) assay kits per the manufacturer's protocol.

For Th1/Th2 assays, human naïve CD4+ T cells were either thawed from frozen stock or freshly isolated. The cells were rested in complete media (RPMI +10% FBS + 1% penicillin/streptomycin + 10 ng/mL IL-2 (Peprotech 200-02)) for at least 2 hours at 37°C /5% CO_2. The cells were then plated at 15,000 cells/well in complete media in a 384-well tissue culture plate. Dynabeads Human T-Activator CD3/CD28 (Invitrogen 11132D) was added to each well at a final concentration of 1 bead/cell. For the Th1 assay a final concentration of 5 ng/mL rhIL-12 (R&D Systems 219-IL/CF) and 5 µg/mL anti-human IL-4 (eBioscience 16-7048-85) were added and for Th2 assay a final concentration of 50 ng/mL rhIL-4 (R&D Systems 204-IL/CF), 10 µg/mL anti-human IFNγ (eBioscience 16-731885) and 5 µg/mL anti-human IL-10 (eBioscience 16-7108-85) were added. Finally, compound/DMSO was added for a final concentration of 0.3% DMSO in a total volume of 100 µL/well and placed in a tissue culture incubator at 37°C / 5% CO_2. On day 7, supernatants were collected and IFNγ (Th1) and IL-13 (Th2) were measured by MSD following the manufacturer's protocol (IFNγ and IL-13 Meso Scale Diagnostics K211AEB-2 and B21UB-3).

For the Th17 assay, human naïve CD4+ T cells were rested in complete media (X-VIVO 15 + 1% P/S) for at least 2 hours at 37°C / 5% CO_2. Meanwhile, a 384-well tissue culture plate was coated with 10 µg/ml anti-human CD3 (eBioscience 16-0037-85) in PBS-CMF for 2 hours at 37°C. The anti-human CD3 was aspirated off the plate and cells were added at a concentration of 20,000 cells/well in complete media. A cytokine skewing cocktail was added with final concentrations of 1000 ng/mL anti-human

CD28 (eBioscience 16-0289-85), 25 ng/mL IL-6 (Peprotech AF-200-06), 5 ng/mL TGFβ1 (Peprotech 100-21), 12.5 ng/mL IL-1β (Peprotech AF-200-01B), 25 ng/mL IL-21, and 25 ng/mL IL-23 (R&D Systems 1290-IL). Finally, compound/DMSO was added for a final concentration of 0.3% DMSO in a total of 100 μL/well and placed in a tissue culture incubator at 37°C / 5% CO_2. On day 6, supernatants were collected and IL-17 measured by MSD following the manufacturer's protocol (IL-17A: Meso Scale Diagnostics K211ATB-2)

The MSD raw data was converted to pg/mL using the standard curve for each plate, and the pg/ml values were converted to percent inhibition. The compound concentrations and percent inhibition values were entered into GraphPad Prism Version 10.4.1 to determine the IC_{50} using a four-parameter fit logistic equation. The IC_{50} reported is the arithmetic mean of the IC_{50} determined for each individual experiment.

Isolated TRKA, TRKB, and TRKC Enzyme Potency

Potency for PF-07245303 inhibition of TRKA, TRKB, and TRKC kinase activity was performed at Carna Biosciences, Inc. Details of this kinase assay method are available in supplemental methods section.

Whole Cell Potency in Cells Expressing Recombinant TRKA, TRKB, TRKC

The cell-based potency of PF-07245303 was determined in vitro at DiscoveRx using their PathHunter® technology which uses an enzyme functional complementation technology. This assay was used to assess the inhibitory effect of PF-07245303 on β-NGF-induced TRKA-, BDNF-induced TRKB-, and NT-3-induced TRKC dependent phosphorylation in cells. Details of this cellular assay method are available in the supplemental methods section.

Whole Cell Potency in Primary Cells Expressing Native TRKA

Fresh human whole blood was collected into sodium heparin anti-coagulant tubes, plated in a 96- deep-well plate and mixed with the compound dilutions prepared as 10-point, 3-fold dilution series to yield final compound concentrations of 30 µM to 0.002 µM with 0.2% DMSO. The mixture was placed in an incubator at 37°C with 5% CO_2 for 30 minutes followed by stimulation with recombinant human NGF (R&D Systems, 256-GF) at a final concentration 0.1 µg/mL (or PBS as negative control) and the resulting mixtures were further incubated for 20 minutes. Next, anti-CD123-APC (Miltenyi Biotec, 130-115-265) and anti-CD203c-PE (Miltenyi Biotec, 130-092-343) antibodies were added and continued to incubate for another 15 minutes. Optilyse B solution (Beckman Coulter, IMI400) was added to each well to lyse the red blood cells and the plate was incubated at room temperature for 10 minutes. Next, distilled water was added to each well and room temperature incubation continued for an additional 10 minutes. The assay plate was centrifuged, and cell pellets were washed and resuspended in PBS. The labeled samples were acquired using LSRFortessa Flow Cytometer (Becton-Dickinson) and analyzed using FlowJo Version 10 from BD. Forward and side scatter was used to gate on all live non-neutrophil cells, then CD123+/CD203c+ cells were gated as activated basophils (Supplemental Figure 6). Compounds were tested in a dose response manner in five different donors, and the data from each experiment were fit to a four-parameter logistic equation to determine IC_{50} values.

Phospho-TRKA Detection in Human Skin Ex Vivo

Freshly excised healthy human abdominal skin from cosmetic reduction surgery was acquired from BioIVT (Westbury, NY). The skin was dermatomed to a thickness of 750 µm before being shipped overnight in skin culture media containing DMEM/F12 with GlutaMax, 180 µM adenine, 0.94 mM calcium chloride, 10 nM 3,3,5 triiodo-L-thyronine, 1X ITS-X, 100x antibiotic/antimycotic, 2% heat-inactivated FBS, 10 µg/ml gentamicin. Seven mm punch biopsies were obtained from the skin and transferred to inserts of a 24 well transwell plate with skin culture media in the bottom. The skin pieces

were cultured at air-liquid surface, with the stratum corneum facing up and exposed to air and the dermis of the section was facing down and exposed to media. IL-4 (20 ng/ml) and IL-13 (20 ng/ml) were added to the skin culture media and plates were transferred to a humidified incubator at 37°C/5% CO_2. After 24 hours, skin pieces were transferred into Eppendorf tubes with or without NGF (10 μg/ml) and compound in DPBS-CMF. Tubes were incubated at 37°C/5% CO_2 for 5 min. Skin tissue was then snap-frozen immediately and stored at -80°C for protein analysis.

Tissue was powderized and homogenized in 1X cell lysis buffer with 1X Halt™ Protease and Phosphatase Inhibitor Cocktail (EDTA-free). Lysates were centrifuged for 15 min at 4°C at maximum speed. Supernatant was collected and quantified using Pierce™ Rapid Gold BCA Protein Assay Kit. Samples were diluted to equal concentrations for pTRKA measurement. An MSD-based assay was performed by using hTRKA mAb (R&D Systems MAB1751R100) as the capture antibody and phospho-TRKA rabbit mAb anti-TRKA (Tyr674/675)/TRKB (Tyr706/707) (C50F3) Rabbit mAb (Cell Signaling 4621S, lot 10) as the detection antibody. Plate was read with MESO SECTOR S 600 instrument.

Ex Vivo Human Skin Model of Atopic Dermatitis

The human abdominal skin was cut using 7 mm biopsy punches and cultured at air-liquid surface. ImmunoCult™ human anti-CD3/CD28 T Cell Activator and DMSO or compounds were simultaneously delivered basolaterally by addition to the skin culture media. After 24 hours incubation, skin tissue was harvested for gene expression analysis and culture media was collected for protein analysis. Skin tissue was minced, lysed in RLT buffer (Qiagen RNeasy Mini kit) containing 1% betamercaptoethanol (Gibco, 21985-023) and homogenized with Bertin Precylls Cryo Evolution. Lysates were centrifuged for 15 min at 4°C at maximum speed. Supernatants were collected for RNA extraction. RNeasy Mini kit (Qiagen 74106) was used to extract RNA following the manufacturer's protocol. RNA was quantified using

BioTek™ Synergy™ H4 Hybrid Microplate Reader. The qPCR assay was carried out in 384-well plates with TaqMan® RNA-to-Ct™ 1-Step Kit. The qPCR reaction was performed in a Quant7 Studio PCR System with the following incubation sequence: 48°C for 15 min, 95°C for 10 min and 40 cycles each of 95°C for 15 seconds and 60°C for 1 min. For results analysis, each sample was normalized to its own TBP internal standard.

The skin culture media (50 µl/well) was analyzed for IL-2 and other proteins using MSD's V-PLEX Human Proinflammatory Panel 1 kit (Meso Scale Diagnostics, K15049D) according to manufacturer's protocols and plates were read on MESO SECTOR S 600. Standards from the kit were used to calculate the concentration of protein levels in the media (Supplemental Table 4).

For topical delivery experiments, human skin explants were freshly obtained from surgical specimens, mounted in Franz cell devices and stimulated with antibodies to CD3 and CD28, which activate the T cell receptor, and a cocktail of Th2 cytokines important for atopic dermatitis pathology. PF-07245303 was formulated in a fit-for-purpose (FFP) vehicle and applied to the apical surface of the skin[54]. Percent activity on *IL2*, *IL13*, *IFNG* and *IL17A* gene expression with vehicle or PF-07245303 treatment relative to Th2 stimulation with no treatment were calculated using three control genes (*GAPDH, RPLP0,* and *ACTB*) for the data analysis (Supplemental Table 6). The following qPCR Taqman probes from Applied Biosystems (Life Technologies) were used: Hs00174114_m1(*IL2*), Hs00174379_m1 (*IL13*), Hs00989291_m1 (*IFNG*), Hs00174383_m1 (*IL17A*), Hs00427620_m2 (*TBP*), Hs02758991_g1 (*GAPDH*), Hs01060665_g1 (*ACTB*), and Hs00420895_gH (*RPLP0*).

RNA Sequencing

The RNA was extracted from skin cultures using isopropanol extraction at MedPharm, Ltd. and sequenced[77]. RNA was sequenced at Fulgent using an Illumina NovaSeq 6000, the TruSeq Stranded mRNA sample preparation kit with 2 × 150 base pair (bp) paired end reads to a mean read depth of 28

million read pairs per sample. Output BCL files were demultiplexed to fastq using Illumina's bcl2fastq2-2.20 tool. The sequencing reads were mapped to the GRCh38 human reference genome using Star v.2.7.3a[78] and subsequently gene counts were generated using Salmon v0.14.2[79]. Transcripts were annotated using Ensemble v98.

Mice

Female BALB/c mice 8-10 weeks of age were obtained from Taconic Biosciences and Charles River Laboratories. All mice were housed in a specific-pathogen-free environment at Pfizer animal facility. Food (2916 Teklad Irradiated Global 16% Protein Rodent diet) and water were provided ad libitum. The vivarium holding rooms were maintained with 12-hour light/dark cycle, 72 °F and 30-70% relative humidity.

Oxazolone-induced Contact Hypersensitivity

Mice were sensitized epicutaneously by application of 100 ml of 4% 4-ethoxymethylene-2-phenyl-2-oxazolin-5-one (oxazolone; SIGMA-Aldrich, St. Louis, MO) diluted in ethanol to the shaved ventral abdomen. Five days later, the mice were challenged by application of 20 µl of 1% oxazolone in ethanol to both sides of the right ear, and 20 µl of vehicle (ethanol) alone to both sides of the left ear at the indicated time points. Ear thickness was measured with an engineering micrometer (Model 7326; Mitutoyo America Corp, IL) at day 0 prior to first challenge (baseline), on each day of the challenge prior to application of oxazolone solution and at the final day of the study. For each timepoint ear swelling was calculated as ear thickness minus baseline value for each ear. One hour after the first challenge and daily after mice received topical 2% PF-07245303 or vehicle applied in 20 µl volume to the front and back of both ears. Twenty-four hours after the last dose, ear skin inflammation was scored using adapted EASI scoring system assessing erythema (redness), induration (thickness) and desquamation (scaling), on a scale of 0-4 each, with maximum score of 16 assigned to each animal. Ears

from half of each treatment group were preserved in 10% neutral buffered formalin (Thermo Fisher) for histological assessment, or flash frozen in liquid nitrogen for tissue cytokine analysis. Methods for microscopic review and scoring can be found in the supplemental methods section. Investigators were blinded to group allocation during data collection and analysis.

Measurement of Cytokines

To measure cytokine levels in ear skin tissue frozen samples were homogenized in T-PER buffer supplemented with protease cocktail (both from Thermo Fisher). Frozen tissue was cut in small fragments with scissors in T-PER/proteinase buffer, then one 5mm stainless steel bead (QIAGEN) was added to each sample tube. Sample tubes were homogenized with TissueLyser II (QIAGEN) and total protein concentration was determined by a BCA assay kit (Pierce) following the manufacturer's protocol. Levels of cytokines in the ear tissue homogenates were determined by MSD kit (U-PLEX T-Cell Combo [mouse], Meso Scale Diagnostics) according to the manufacturer's instructions. All values were normalized to the total protein concentration per sample.

Statistical Analysis

For analysis of the p-TrkA ex vivo skin assay, all data points were subtracted by the average unstimulated values and then divided by the average stimulated (IL-4, IL-13 and NGF) values to normalize. A one way ANOVA model was utilized with normalized expression as the response variable and treatment as the fixed effect. The model was fit by the lm function in R version 3.5. The least square mean estimates, the estimates of the treatment differences compared to vehicle, and fold change was determined. Adjusted multiple comparison p-values with the FDR method. Notable inhibition was defined as $p < 0.05$ and $F < -0.5$.

In the statistical analysis of the ex vivo human skin model of AD, a linear mixed model was fit with $\Delta\Delta Ct$ as the response variable, donor as random effect, and treatment as the fixed effect with or without

heterogenous variance for the treatments or a one-way ANOVA. The model was fit by the lme function with the restricted maximum likelihood or lm function in R version 3.5. The least square mean estimates and the estimates of the treatment differences compared to vehicles were determined. Adjusted multiple comparison p-values with the false discovery rate (FDR) method. The adjustment to the p-values was based on 3 or 4 comparisons, gene expression and protein, respectively. The % inhibition for gene expression was calculated using the formula: $(1-F)*100\%$. F is the fold change which equals $2^{-\text{estimated } \Delta\Delta Ct \text{ Treatment Difference}}$.

RNAseq gene expression was normalized using edgeR package[80] and gene expression differences were evaluated using limma R package[81]. The P-values were corrected for multiple hypothesis testing using the Benjamini-Hochberg false discovery rate[82,81]. All analysis were implemented in R version 4.2.1 and all visualizations were created using the EnhancedVolcanoplot R package version 1.14.0 or ggplot2 R package version 4.0.0[83].

In the statistical analysis of mouse ear thickness, a linear mixed model was fit with ear thickness as the response variable, donor as random effect, and treatment as the fixed effect with heterogenous variance for the treatments. The model was fit by the lme function with the restricted maximum likelihood in R version 3.5. The least square mean estimates and the estimates of the treatment differences compared to vehicles were determined. Adjusted multiple comparison p-values with the false discovery rate (FDR) method. The adjustment to the p-values was based on 2 comparisons.

Data Availability

Source Data has been provided and all primary data generated for this study will be readily shared with researchers for reproducibility purposes upon request. The diffraction data and coordinates of ITK bound to PF-07245303 compound have been deposited in the Protein Data Bank (PDB) under the

accession code 9NWX. The RNA sequencing data generated has been deposited in the GEO repository under accession code GSE297645.

References

1. Brunner, P. M., Guttman-Yassky, E. & Leung, D. Y. The immunology of atopic dermatitis and its reversibility with broad-spectrum and targeted therapies. *J. Allergy Clin. Immunol.* **139**, S65–S76 (2017).

2. Brar, K. K., Nicol, N. H. & Boguniewicz, M. Strategies for Successful Management of Severe Atopic Dermatitis. *J. Allergy Clin. Immunol.: Pr.* **7**, 1–16 (2019).

3. Otsuka, A. *et al.* The interplay between genetic and environmental factors in the pathogenesis of atopic dermatitis. *Immunol. Rev.* **278**, 246–262 (2017).

4. Sabat, R., Wolk, K., Loyal, L., Docke, W. D. & Ghoreschi, K. T cell pathology in skin inflammation. *Semin. Immunopathol.* **41**, 359–377 (2019).

5. Sahu, N. & August, A. ITK inhibitors in inflammation and immune-mediated disorders. *Curr. Top. Med. Chem.* **9**, 690–703 (2009).

6. Andreotti, A. H., Schwartzberg, P. L., Joseph, R. E. & Berg, L. J. T-cell signaling regulated by the Tec family kinase, Itk. *Cold Spring Harb. Perspect. Biol.* **2**, a002287 (2010).

7. Felices, M., Falk, M., Kosaka, Y. & Berg, L. J. Tec Kinases in T Cell and Mast Cell Signaling. in vol. 93 145–184 (2007).

8. Au-Yeung, B. B., Katzman, S. D. & Fowell, D. J. Cutting edge: Itk-dependent signals required for CD4+ T cells to exert, but not gain, Th2 effector function. *J. Immunol.* **176**, 3895–9 (2006).

9. Lin, T. A. *et al.* Selective Itk inhibitors block T-cell activation and murine lung inflammation. *Biochemistry* **43**, 11056–62 (2004).

10. Andreotti, A. H., Joseph, R. E., Conley, J. M., Iwasa, J. & Berg, L. J. Multidomain Control Over TEC Kinase Activation State Tunes the T Cell Response. *Annu. Rev. Immunol.* **36**, 549–578 (2018).

11. August, A. & Ragin, M. J. Regulation of T-cell responses and disease by tec kinase Itk. *Int. Rev. Immunol.* **31**, 155–65 (2012).

12. Weeks, S., Harris, R. & Karimi, M. Targeting ITK signaling for T cell-mediated diseases. *iScience* **24**, 102842 (2021).

13. Ferrara, T. J., Mueller, C., Sahu, N., Ben-Jebria, A. & August, A. Reduced airway hyperresponsiveness and tracheal responses during allergic asthma in mice lacking tyrosine kinase inducible T-cell kinase. *J. Allergy Clin. Immunol.* **117**, 780–6 (2006).

14. Jain, N. *et al.* CD28 and ITK signals regulate autoreactive T cell trafficking. *Nat. Med.* **19**, 1632–7 (2013).

15. Mueller, C. & August, A. Attenuation of immunological symptoms of allergic asthma in mice lacking the tyrosine kinase ITK. *J. Immunol.* **170**, 5056–63 (2003).

16. Lechner, K. *et al.* Targeting of the Tec Kinase ITK Drives Resolution of T Cell-Mediated Colitis and Emerges as Potential Therapeutic Option in Ulcerative Colitis. *Gastroenterology* **161**, 1270-1287 e19 (2021).

17. Kannan, A. K., Kim, D. G., August, A. & Bynoe, M. S. Itk signals promote neuroinflammation by regulating CD4+ T-cell activation and trafficking. *J. Neurosci.* **35**, 221–33 (2015).

18. Gomez-Rodriguez, J. *et al.* Itk is required for Th9 differentiation via TCR-mediated induction of IL-2 and IRF4. *Nat. Commun.* **7**, 10857 (2016).

19. Deakin, A. *et al.* Characterisation of a K390R ITK kinase dead transgenic mouse--implications for ITK as a therapeutic target. *PLoS ONE* **9**, e107490 (2014).

20. Bonin, A. von *et al.* Inhibition of the IL-2-inducible tyrosine kinase (Itk) activity: a new concept for the therapy of inflammatory skin diseases. *Exp. Dermatol.* **20**, 41–7 (2011).

21. Otake, S. *et al.* Topical Application of BMS-509744, a Selective Inhibitor of Interleukin-2-Inducible T Cell Kinase, Ameliorates Imiquimod-Induced Skin Inflammation in Mice. *Biol. Pharm. Bull.* **44**, 528–534 (2021).

22. Nadeem, A. *et al.* Inhibition of interleukin-2-inducible T-cell kinase causes reduction in imiquimod-induced psoriasiform inflammation through reduction of Th17 cells and enhancement of Treg cells in mice. *Biochimie* **179**, 146–156 (2020).

23. Sun, Y. *et al.* Inhibition of the kinase ITK in a mouse model of asthma reduces cell death and fails to inhibit the inflammatory response. *Sci. Signal.* **8**, ra122 (2015).

24. Matsumoto, Y. *et al.* Identification of highly expressed genes in peripheral blood T cells from patients with atopic dermatitis. *Int. Arch. Allergy Immunol.* **129**, 327–40 (2002).

25. Kannan, A. *et al.* Allele-sensitive mutant, Itkas, reveals that Itk kinase activity is required for Th1, Th2, Th17, and iNKT-cell cytokine production. *Eur. J. Immunol.* **45**, 2276–85 (2015).

26. Mollanazar, N. K., Smith, P. K. & Yosipovitch, G. Mediators of Chronic Pruritus in Atopic Dermatitis: Getting the Itch Out? *Clin. Rev. Allergy Immunol.* **51**, 263–292 (2016).

27. Benecke, H., Lotts, T. & Stander, S. Investigational drugs for pruritus. *Expert Opin. Investig. Drugs* **22**, 1167–79 (2013).

28. Botchkarev, V. A. *et al.* Neurotrophins in skin biology and pathology. *J. Investig. Dermatol.* **126**, 1719–27 (2006).

29. Rukwied, R. R., Main, M., Weinkauf, B. & Schmelz, M. NGF sensitizes nociceptors for cowhage- but not histamine-induced itch in human skin. *J. Investig. Dermatol.* **133**, 268–70 (2013).

30. Yamaguchi, J., Aihara, M., Kobayashi, Y., Kambara, T. & Ikezawa, Z. Quantitative analysis of nerve growth factor (NGF) in the atopic dermatitis and psoriasis horny layer and effect of treatment on NGF in atopic dermatitis. *J. Dermatol. Sci.* **53**, 48–54 (2009).

31. Matsumura, S., Terao, M., Murota, H. & Katayama, I. Th2 cytokines enhance TrkA expression, upregulate proliferation, and downregulate differentiation of keratinocytes. *J. Dermatol. Sci.* **78**, 215–23 (2015).

32. Tominaga, M., Tengara, S., Kamo, A., Ogawa, H. & Takamori, K. Psoralen-ultraviolet A therapy alters epidermal Sema3A and NGF levels and modulates epidermal innervation in atopic dermatitis. *J. Dermatol. Sci.* **55**, 40–6 (2009).

33. Bürgi, B. *et al.* Basophil priming by neurotrophic factors. Activation through the trk receptor. *J Immunol* **157**, 5582–8 (1996).

34. Bischoff, S. C. & Dahinden, C. A. Effect of nerve growth factor on the release of inflammatory mediators by mature human basophils. *Blood* **79**, 2662–9 (1992).

35. Bryan, M. C. & Rajapaksa, N. S. Kinase Inhibitors for the Treatment of Immunological Disorders: Recent Advances. *J. Med. Chem.* **61**, 9030–9058 (2018).

36. Zapf, C. W. *et al.* Covalent inhibitors of interleukin-2 inducible T cell kinase (itk) with nanomolar potency in a whole-blood assay. *J. Med. Chem.* **55**, 10047–63 (2012).

37. Han, S. *et al.* Selectively targeting an inactive conformation of interleukin-2-inducible T-cell kinase by allosteric inhibitors. *Biochem. J.* **460**, 211–22 (2014).

38. Proschak, E., Stark, H. & Merk, D. Polypharmacology by Design: A Medicinal Chemist's Perspective on Multitargeting Compounds. *J. Med. Chem.* **62**, 420–444 (2019).

39. Roberts, M. S. *et al.* Topical drug delivery: History, percutaneous absorption, and product development. *Adv. Drug Deliv. Rev.* **177**, 113929 (2021).

40. Di, L. *et al.* Development of a new permeability assay using low-efflux MDCKII cells. *J. Pharm. Sci.* **100**, 4974–4985 (2011).

41. Aprile, S., Serafini, M. & Pirali, T. Soft drugs for dermatological applications: recent trends. *Drug Discov. Today* **24**, 2234–2246 (2019).

42. Ryu, S. *et al.* Evaluation of Fraction Unbound Across 7 Tissues of 5 Species. *J. Pharm. Sci.* **109**, 1178–1190 (2020).

43. Yu, S. *et al.* A novel liquid chromatography/tandem mass spectrometry based depletion method for measuring red blood cell partitioning of pharmaceutical compounds in drug discovery. *Rapid Commun. Mass Spectrom.* **19**, 250–254 (2005).

44. Bagal, S. K. *et al.* Discovery of Potent, Selective, and Peripherally Restricted Pan-Trk Kinase Inhibitors for the Treatment of Pain. *J. Med. Chem.* **61**, 6779–6800 (2018).

45. Rashighi, M. & Harris, J. E. Vitiligo Pathogenesis and Emerging Treatments. *Dermatol. Clin.* **35**, 257–265 (2017).

46. Olayinka, J. J. T. & Richmond, J. M. Immunopathogenesis of alopecia areata. *Curr. Res. Immunol.* **2**, 7–11 (2021).

47. Ito, Y. *et al.* Basophil recruitment and activation in inflammatory skin diseases. *Allergy* **66**, 1107–13 (2011).

48. Bürgi, B. *et al.* Basophil priming by neurotrophic factors. Activation through the trk receptor. *J Immunol* **157**, 5582–8 (1996).

49. Lourenço, F. D. *et al.* Activated status of basophils in chronic urticaria leads to interleukin-3 hyper-responsiveness and enhancement of histamine release induced by anti-IgE stimulus. *Br. J. Dermatol.* **158**, 979–86 (2008).

50. Borriello, F., Granata, F. & Marone, G. Basophils and skin disorders. *J. Investig. Dermatol.* **134**, 1202–1210 (2014).

51. Yan, W. *et al.* Insights into Current Tropomyosin Receptor Kinase (TRK) Inhibitors: Development and Clinical Application. *J. Med. Chem.* **62**, 1731–1760 (2019).

52. Price, E. A., Krasowska-Zoladek, A., Nanda, K. K., Stachel, S. J. & Henze, D. A. Development of a pharmacodynamic biomarker to measure target engagement from inhibition of the NGF-TrkA pathway. *J. Neurosci. Methods* **282**, 34–42 (2017).

53. Smith, S. H. *et al.* Development of a Topical Treatment for Psoriasis Targeting RORgamma: From Bench to Skin. *PLoS ONE* **11**, e0147979 (2016).

54. Jones, P. *et al.* Design and Synthesis of a Pan-Janus Kinase Inhibitor Clinical Candidate (PF-06263276) Suitable for Inhaled and Topical Delivery for the Treatment of Inflammatory Diseases of the Lungs and Skin. *J. Med. Chem.* **60**, 767–786 (2017).

55. Brunner, P. M. *et al.* Early-onset pediatric atopic dermatitis is characterized by T(H)2/T(H)17/T(H)22-centered inflammation and lipid alterations. *J. Allergy Clin. Immunol.* **141**, 2094–2106 (2018).

56. Choi, J. *et al.* Translational Relevance of Mouse Models of Atopic Dermatitis. *J. Clin. Med.* **10**, 613 (2021).

57. Guttman-Yassky, E. *et al.* Dupilumab progressively improves systemic and cutaneous abnormalities in patients with atopic dermatitis. *J. Allergy Clin. Immunol.* **143**, 155–172 (2019).

58. Patrick, G. J., Archer, N. K. & Miller, L. S. Which Way Do We Go? Complex Interactions in Atopic Dermatitis Pathogenesis. *J. Investig. Dermatol.* **141**, 274–284 (2021).

59. Guttman-Yassky, E. & Krueger, J. G. Atopic dermatitis and psoriasis: two different immune diseases or one spectrum? *Curr. Opin. Immunol.* **48**, 68–73 (2017).

60. Lechner, K. S., Neurath, M. F. & Weigmann, B. Role of the IL-2 inducible tyrosine kinase ITK and its inhibitors in disease pathogenesis. *J. Mol. Med.* **98**, 1385–1395 (2020).

61. Riether, D. *et al.* 5-Aminomethylbenzimidazoles as potent ITK antagonists. *Bioorg. Med. Chem. Lett.* **19**, 1588–91 (2009).

62. Trani, G. *et al.* Design, synthesis and structure-activity relationships of a novel class of sulfonylpyridine inhibitors of Interleukin-2 inducible T-cell kinase (ITK). *Bioorg. Med. Chem. Lett.* **24**, 5818–5823 (2014).

63. Burch, J. D. *et al.* Tetrahydroindazoles as Interleukin-2 Inducible T-Cell Kinase Inhibitors. Part II. Second-Generation Analogues with Enhanced Potency, Selectivity, and Pharmacodynamic Modulation in Vivo. *J. Med. Chem.* **58**, 3806–16 (2015).

64. Zhong, Y. *et al.* Targeting interleukin-2-inducible T-cell kinase (ITK) and resting lymphocyte kinase (RLK) using a novel covalent inhibitor PRN694. *J. Biol. Chem.* **290**, 5960–78 (2015).

65. Zhou, D., Zuo, Y. & Pan, Z. Discovery of Potent and Highly Selective Interleukin-2-Inducible T-Cell Kinase Degraders with In Vivo Activity. *J. Med. Chem.* **66**, 4979–4998 (2023).

66. Hsu, L.-Y. *et al.* Synthesis and characterization of soquelitinib a selective ITK inhibitor that modulates tumor immunity. *npj Drug Discov.* **1**, 2 (2024).

67. Colgan, J. D. & Hankel, I. L. Signaling pathways critical for allergic airway inflammation. *Curr. Opin. Allergy Clin. Immunol.* **10**, 42–7 (2010).

68. Gomez-Rodriguez, J. *et al.* Differential expression of interleukin-17A and -17F is coupled to T cell receptor signaling via inducible T cell kinase. *Immunity* **31**, 587–97 (2009).

69. Gomez-Rodriguez, J. *et al.* Itk-mediated integration of T cell receptor and cytokine signaling regulates the balance between Th17 and regulatory T cells. *J. Exp. Med.* **211**, 529–43 (2014).

70. Neil, J. E., Brown, M. B. & Williams, A. C. Human skin explant model for the investigation of topical therapeutics. *Sci. Rep.* **10**, 21192 (2020).

71. Takano, N., Sakurai, T., Ohashi, Y. & Kurachi, M. Effects of high-affinity nerve growth factor receptor inhibitors on symptoms in the NC/Nga mouse atopic dermatitis model. *Br. J. Dermatol.* **156**, 241–6 (2007).

72. Roblin, D. *et al.* Topical TrkA Kinase Inhibitor CT327 is an Effective, Novel Therapy for the Treatment of Pruritus due to Psoriasis: Results from Experimental Studies, and Efficacy and Safety of CT327 in a Phase 2b Clinical Trial in Patients with Psoriasis. *Acta Derm. Venereol.* **95**, 542–8 (2015).

73. Kleinman, E., Laborada, J., Metterle, L. & Eichenfield, L. F. What's New in Topicals for Atopic Dermatitis? *Am. J. Clin. Dermatol.* **23**, 595–603 (2022).

74. Wang, F. *et al.* A basophil-neuronal axis promotes itch. *Cell* **184**, 422-440.e17 (2021).

75. Sin, A. Z., Roche, E. M., Togias, A., Lichtenstein, L. M. & Schroeder, J. T. Nerve growth factor or IL-3 induces more IL-13 production from basophils of allergic subjects than from basophils of nonallergic subjects. *J. Allergy Clin. Immunol.* **108**, 387–93 (2001).

76. Simpson, E. L. *et al.* Efficacy and Safety of Dupilumab in Adolescents With Uncontrolled Moderate to Severe Atopic Dermatitis: A Phase 3 Randomized Clinical Trial. *JAMA Dermatol.* **156**, 44–56 (2020).

77. Folkersen, L. *et al.* Integration of known DNA, RNA and protein biomarkers provides prediction of anti-TNF response in rheumatoid arthritis: results from the COMBINE study. *Mol. Med.* **22**, 322–328 (2016).

78. Dobin, A. *et al.* STAR: ultrafast universal RNA-seq aligner. *Bioinformatics* **29**, 15–21 (2013).

79. Patro, R., Duggal, G., Love, M. I., Irizarry, R. A. & Kingsford, C. Salmon provides fast and bias-aware quantification of transcript expression. *Nat. Methods* **14**, 417–419 (2017).

80. Chen, Y., Chen, L., Lun, A. T. L., Baldoni, P. L. & Smyth, G. K. edgeR v4: powerful differential analysis of sequencing data with expanded functionality and improved support for small counts and larger datasets. *Nucleic Acids Res.* **53**, gkaf018 (2025).

81. Ritchie, M. E. *et al.* limma powers differential expression analyses for RNA-sequencing and microarray studies. *Nucleic Acids Res.* **43**, e47 (2015).

82. Benjamini, Y. & Hochberg, Y. Controlling the False Discovery Rate: A Practical and Powerful Approach to Multiple Testing. *J. R. Stat. Soc.: Ser. B (Methodol.)* **57**, 289–300 (1995).

83. Wickham, H. *Ggplot2 Elegant Graphics for Data Analysis*. (Springer New York, 2009). doi:10.1007/978-0-387-98141-3.

84. Keefer, C. *et al.* Mechanistic insights on clearance and inhibition discordance between liver microsomes and hepatocytes when clearance in liver microsomes is higher than in hepatocytes. *Eur. J. Pharm. Sci.* **155**, 105541 (2020).

85. Goetz, A. E. *et al.* Demonstration of a Multikilogram-Scale Birch Reduction and Evaluation of Alternative Synthetic Routes to a Ketalized Cyclohexene Derivative. *Org. Process Res. Dev.* (2023) doi:10.1021/acs.oprd.3c00141.

Acknowledgements:

We thank the staff of the Pfizer Flow Cytometry and Next-Generation Sequencing Technology Centers for their support. We thank Alexia Scaros and Ying Zhang for outsourcing support. We thank Isac Lee and Samir Lal with assistance with the submission of the RNAseq gene expression data and figure formatting.

Author Contributions

A.L.B., K.F. L.J., J.B., J.H.S., K.K.C., C.A., Y.Z., T.A., R.T.S., W.L., A.R., J.V. performed biochemical, cell-based, ex vivo skin experiments or in vivo study, analyzed the data, and prepared the methods sections. K.H. performed microscopic analysis of tissue sections from in vivo model. N.L.N., S.L. performed crystallography studies and determined the structures. J.E.D., J.W.S., A.C-G., G.M.C., F.E.L., R.A.D., S.D., R.H., M.P., J.I.T., S.W.B., B.S.G. designed and synthesized PF-07245303. S.A.J., Y.L. conducted transcriptomics and the corresponding quantitative analysis and data visualization. J.G. and S.A.J. performed statistical analysis. J.L.D., S.J., T.L.F., S.J.S., K.N., M.H., F.V., K.L.L. B.S.G., and M.J.P. were involved in the experimental design and data interpretation. J.L.D., S.W.J., J.B., S.L., S.W.B., B.S.G, and M.J.P. wrote the manuscript with input from all authors.

Corresponding authors

Correspondence should be addressed to J.L.D. (email: Jennifer.Duffen@pfizer.com) or B.S.G. (email: Brian.Gerstenberger@pfizer.com).

Competing Interests

J.L.D., K.K.C. L.J., A.B., K.F., J.B., S.J., Y.L., J.H.S., Y.Z. T.A., K.H., C.A., R.T.S., J.G., S.B., A.C-G, G.C., J.D., R.A.D, S.D., T.F., R.W.H., S.L., F.L., N.N., M.P., J.S., J.I.T., S.S., K.N., M.H., F.V., K.L.L., B.S.G., and M.J.P. were employees of Pfizer Inc. at the time this work was performed. W.L., A.R., J.V. were employees of MedPharm Ltd. at the time this work was performed. The authors declared no other competing interests.

FIGURE 1. Profile of PF-07245303. a Structure of PF-07245303. **b** PF-07245303 co-crystal structure with ITK protein identifying binding sites and docking mode to ITK ATP catalytic site at 1.35 Å (PDB 9NWX). **c** PF-07245303 binding kinetics to recombinant ITK, TRKA, TRKB and TRKC protein using SPR. **d** In vitro absorption, distribution, metabolism, and excretion profile for PF-07245303. **e** Kinome selectivity for PF-07245303 tested at 1 µM. against a panel of 218 kinase constructs colored by present inhibition in a biochemical assays using 1 mM ATP

FIGURE 2. Evaluation of PF-07245303 effects on ITK kinase activity, proximal ITK signaling in cells, and IL-2 release from stimulated CD4+ T cells or stimulated human whole blood. a Effect of PF-07245303 on in vitro biochemical kinase activity of human full-length ITK enzyme in the presence of 1 mM ATP. Percent inhibitions are determined for a range of concentrations of PF-07245303. Graph of mean % inhibition ± SD at each concentration across n = 13 experiments. **b** Measurement of ITK-dependent phosphorylation of PLCγ1 induced by anti-CD3 and anti-CD28 antibody activation of Jurkat T cells. Total PLCγ1 and phosphorylated PLCγ1 were detected in whole cell lysates with immunoblotting. Graph of mean % inhibition of PLCγ1 phosphorylation using densitometry measurement of imunoblots for a range of concentrations of PF-07245303. One representative immunoblot and graph of mean % inhibition ± SD for n = 4 experiments. **c-d** Percent inhibition curves for PF-07245303 measuring IL-2 release from **c** isolated naïve, human CD4+ T cells stimulated with anti-CD3 and anti-CD28 antibodies or **d** T cells in human blood stimulated with anti-CD3, anti-CD28, and anti-CD2 antibodies. Graph of mean % inhibition ± SD at each concentration across n = 14 experiments for both isolated T cells and whole blood.

FIGURE 3. Effect of PF-07245303 on cytokine release from TCR-activated naïve CD4+ T cells, differentiated human Th1, Th2, and Th17 cells. a-e PF-07245303 inhibits cytokine release from naïve,

human T cells. Concentration-dependent inhibition of **a** IL-4, **b** IL-13, **c** IFNγ, **d** IL-17A, **e** IL-10 from anti-CD3 and anti-CD28 stimulated T cells treated with PF-07245303. T cells from 2 different donors were tested and mean percent inhibitions for duplicates at each concentration are shown. **f-h** PF-07245303 inhibited the release of IFNγ, IL-13, and IL-17 from human naïve CD4+ T cells stimulated with anti-CD3, anti-CD28 antibodies and cytokine cocktails to generate T cells skewed to **f** Th1, **g** Th2 and **h** Th17 T cells. T cells from 4 different donors **f** and **g** and 2 different donors **h** were tested and average percent inhibitions for triplicates at each concentration ± SD are shown.

FIGURE 4. PF-07245303 inhibits TRK kinase activity and TRK-dependent signaling in cells, blood basophils, and skin explants. a-c Effects of PF-07245303 on kinase activity of human **a** TRKA, **b** TRKB, and **c** TRKC were determined. Graphs of mean % inhibition ± SD at each concentration **a** n = 5 experiments and **b,c** n = 4 experiments. **d-f** PF-07245303 inhibits **d** TRKA, **e** TRKB, and **f** TRKC-dependent phosphorylation in cells expressing human TRKA, TRKB or TRKC and p75. Ligand-induced receptor activation is detected by receptor phosphorylation-induced functional complementation and restored β-galactosidase activity measured by chemiluminescence. Inhibition of **d** TRKA, **e** TRKB, and **f** TRKC activation with PF-07245303 or selective pan-TRK inhibitor PF-06273340. **d-f** Graph of mean % inhibition ± SD at each concentration across n = 4 experiments. **g** Determination of PF-07245303 inhibition of TRKA in human blood basophils. Graph of mean % inhibition ± SD of NGF-induced increase in the percent of basophils double positive for CD123 and CD203c at each concentration of PF-07245303 or PF-06273340 across n = 5 donors. **h** NGF-induced TRKA phosphorylation was measured in human skin sections treated with PF-07245303 (10 μM to 0.1 μM) or with 10 μM of PF-06273340 and stimulated with NGF. Representative results for phospho-TRKA activation and mean % inhibition ± SD in skin from one donor. Skin from 3 donors with 6 replicates per condition was evaluated. Comparisons of mean differences=Δ versus control is done by t-test with 113 degrees of freedom and FDR adjusted two-sided p-values. 0.1 μM has a Δ=-26.5 a t=-2.28 and p-value=0.0244. 0.3 μM has a Δ=-49.8 a t=-4.78 and p-value=6.58e-06. 1 μM has a Δ=-74.6 a t=-7.18 and p-value=1.34e-10. 3 μM has a Δ=-86.6 a t=-8.33 and p-value=5.44e-13. 10 μM has a Δ=-93.2 a t=-8.96 and p-value=3.91e-14. Notable changes in phospho-TRKA levels relative to vehicle were defined as $p < 0.0001$ and $F < -0.50$ and denoted with ***. $F=2^{-\text{estimated } \Delta\Delta Ct \text{ Treatment Difference}}$ and F and F 95% CI are in supplementary table 4.

FIGURE 5. PF-07245303 inhibits activation of resident dermal T cells in ex vivo human skin sections stimulated with anti-CD3 and anti-CD28 antibodies. Treatment of human ex vivo skin

sections with anti-CD3 and anti-CD28 antibodies induced expression of **a** *IFNG*, **b** *IL13*, and **c** *IL2* transcript measured in tissue lysates and **d** IL-2 protein in culture media at 24 hours post-stimulation. Graphs of mean expression ± SD from skin tissue from one donor representative of the results using skin from 3 different donors. Increasing concentrations of PF-07245303 inhibited **a** *IFNG*, **b** *IL13*, and **c** *IL2* expression in ex vivo skin sections stimulated by anti-CD3 and anti-CD28 antibodies. **d** Concentration-dependent inhibition of IL-2 production was observed with PF-07245303 added to the culture media. Graphs of mean pg/ml IL-2 ± SD at each concentration of compound. **a-d** Comparisons of mean differences=Δ versus control is done by t-test (b (83 degrees of freedom), c (82 degrees of freedom), d (75 degrees of freedom)) or z-test (a) with FDR adjusted two-sided p-values. **a** 1 μM has Δ=0.7544, z=1.903, and p-value=0.0571. 3 μM has Δ=1.7558. z=1.7558. and p-value=2.85e-05. 10 μM has Δ=2.5804, z=4.116, and p-value=5.78e-05. **b** 1 μM has Δ=0.611, t=1.248, and p-value=0.2155. 3 μM has Δ=1.712, t=3.497, and p-value=0.0011. 10 μM has Δ=3.301, t=3.301, and p-value=5.77e-09. **c** 1 μM has Δ=0.983, t=3.801, and p-value=0.0003. 3 μM has Δ=1.007, t=3.833, and p-value=0.0003. 10 μM has Δ=1.501, t=5.803, and p-value=3.56e-07. **d** 0.3 μM has Δ=-4.49, t=-1.031, and p-value=0.3061. 1 μM has Δ=-11.10, t=-2.631, and p-value=0.0138. 3 μM has Δ=-13.68, t=-3.310, and p-value=0.0029. 10 μM has Δ=-14.40, t=-3.483, and p-value=0.0029. **a-c** Statistically significant changes in mRNA levels relative to vehicle control were defined as $p < 0.0001$ denoted with ###, $p < 0.001$ denoted with ##, and $p < 0.01$ denoted with #. **d** Notable changes in IL-2 protein levels relative to vehicle were defined as $p < 0.01$ and $F < -0.50$ denoted with ** and $p < 0.05$ and $F < -0.50$ denoted with *. $F=2^{-\text{estimated } \Delta\Delta Ct \text{ Treatment Difference}}$ and F and F 95% CI are in supplementary table 5.

FIGURE 6. Summary of results for effects of topically applied PF-07245303. Human skin explants were freshly obtained from surgical specimens, mounted in Franz cell devices and stimulated with antibodies to CD3 and CD28 and a cocktail of Th2 cytokines. PF-07245303 was formulated in a fit-for-

purpose (FFP) formulation at 0.2% and 1% concentrations and applied topically to the apical surface of the skin. Gene expression with FFP vehicle or PF-07245303 treatment relative to Th2 stimulation with no treatment were calculated for **a** *IL2*, **b** *IL13*, **c** *IFNG*, and **d** *IL17A* (0.2% PF-07245303, n = 2 donors; 1.0% PF-07245303, n = 5 donors). For box-and-whisker plots, median = center line, box limits = upper and lower quartiles; whiskers = range. **a-d** Comparisons of mean differences is done by t-test with FDR adjusted two-sided p-values. **a** 0.2% versus FFP has a mean difference=2.80 with a t=2.855 and 422 degrees of freedom and a p-value=0.0090. 1% versus FFP has a mean difference=1.88 with a t=2.101 and 422 degrees of freedom and a p-value=0.0362. **b** 0.2% versus FFP has a mean difference=1.89 with a t=1.675 and 422 degrees of freedom and a p-value=0.0947. 1% versus FFP has a mean difference=2.38 with a t=2.298 and 422 degrees of freedom and a p-value=0.0441. **c** 0.2% versus FFP has a mean difference=3.06 with a t=3.265 and 422 degrees of freedom and a p-value=0.0012. 1% versus FFP has a mean difference=3.06 with a t=3.399 and 422 degrees of freedom and a p-value=0.0012. **d** 0.2% versus FFP has a mean difference=1.94 with a t=1.977 and 422 degrees of freedom and a p-value=0.0487. 1% versus FFP has a mean difference=2.08 with a t=2.005 and 422 degrees of freedom and a p-value=0.0487. The % inhibition for gene expression was calculated using the formula: $(1-F)*100\%$. F is the fold change which equals $2^{-\text{estimated } \Delta\Delta\text{Ct Treatment Difference}}$. Statistical significance is denoted by * $p < 0.05$ compared to the FFP vehicle. F and 95% CI are in supplementary table 6.

FIGURE 7. Similarities in gene signatures of differentially expressed genes in a human skin explant model with similar signatures to that found in skin lesions from atopic dermatitis patients. Treatment of skin explants with PF-07245303 can reverse the disease signature. a,b Scatterplot of RNA expression differences in anti-CD3/CD28 and Th2 cytokine-stimulated and unstimulated skin explants. Each dot represents a distinct gene. **a** Red dots represent genes that are induced by stimulation

with p-value < 0.05 and blue dots represent genes that are reduced by stimulation with p-value < 0.05. **b** Dots are colored based on regulation in atopic dermatitis skin tissue versus healthy control from GEO dataset GSE121212. **c** Scatterplot of RNA expression differences in skin explants treated with PF-07245303 and then stimulated with anti-CD3/CD28 and Th2 cytokines. Dots are colored based on the regulation in **a**. **d** Expression of RNA in untreated (n=12), anti-CD3/CD28/Th2 stimulated (n=12), anti-CD3/CD28/Th2/PF-07245303 (n=12) treated skin explants for *CXCL11*, *IFNG*, *IL13*, *IL4*, *IL17A*, *IL2*, *FLG*, *FLG2*, *IL31RA*, *NGF*, *OSMR* and *IL4R* from RNA sequencing studies. Values on the y-axis represent EdgeR normalized expression. Comparisons used Dunn's tests and p-values are adjusted for multiple comparisons using the Holm-Bonferroni method. Data are presented as box plots (centre line at the median, upper bound at 75th percentile, lower bound at 25th percentile) with whiskers at minimum and maximum values. Each dot represents one donor with 3 technical replicates per donor. Source data are provided as a Source Data file.

FIGURE 8. PF-07245303 treatment reduces ear thickness, ear tissue cytokines, and disease severity score in a mouse model of oxazolone-induced dermatitis. a-j Mice were sensitized with 4% oxazolone applied to the abdomen at day -5 and challenged with 1% oxazolone on the right ear or ethanol alone on the left ear on days indicated by arrows. **a** Ear swelling was measured on days of oxazolone challenge and at study completions on day 11 for mice treated with topical application of 2% PF-07245303 (n=15) or topical ethanol (EtOH) vehicle application (n=13). Data are mean ± standard error of the mean. Comparisons of mean differences=Δ versus control is done by t-test with 75.1 or 115.7 degrees of freedom (Oxa or EtOH, respectively) and FDR adjusted two-sided p-values. At t=0, 2% + Oxa Δ=0, t=0, and p-value=1 and 2% + EtOH Δ=0, t=0, and p-value=1. At t=2, 2% + Oxa Δ=-18.21, t=-1.038, and p-value=0.4468 and 2% + EtOH Δ=6.30, t=0.765, and p-value=0.4468. At t=4, 2% + Oxa Δ=-75.99, t=-4.334, and p-value=6.29e-05 and 2% + EtOH Δ=-11.42, t=-1.386, and p-value=0.1699. At t=7, 2% + Oxa Δ=-134.54, t=-7.673, and p-value=1.16e-11 and 2% + EtOH Δ=1.76, t=0.213, and p-value=0.8317. At t=9, 2% + Oxa Δ=-242.13, t=-13.809, and p-value=6.40e-26 and 2% + EtOH Δ=-11.64, t=-1.413, and p-value=0.1619. At t=11, 2% + Oxa Δ=-234.79, t=-13.390, and p-value=5.80e-25 and 2% + EtOH Δ=-6.93, t=-0.841, and p-value=0.4032. **** p <0.0001 **b-f** Histological analysis of ear sections stained with H&E. **b, c** Inflammatory cell infiltrates in the dermis and epithelial changes were scored as described in methods. The sum of scores for inflammatory cell infiltrate and epidermal endpoints for each mouse were plotted. Statistical significance determined by **b, c** Welch's two-tailed t test. **d–f** Representative images of H&E stained ear sections from **d** ethanol and vehicle treated mouse, **e** oxazolone and vehicle treated mouse, and **f** oxazolone and PF-07245303-treated mouse. **g–j** Measurements of cytokine levels detected in ear tissue homogenate, normalized to total protein and expressed as µg/mg of total protein. Statistical significance was determined by Welch's t-test. **b-j** * p <0.05, **p < 0.01, *** p <0.001, **** p <0.0001

Editorial Summary:

Atopic dermatitis is an immune disease driven by cytokines including IL-4/IL-13. This study shows that a topical ITK/TRK inhibitor blocks an array of T cell cytokines, inhibits NGF-induced basophil activation, and reduces inflammation in human skin explants and dermatitis models, indicating therapeutic potential.

Peer Review Information: *Nature Communications* thanks Asier Unciti-Broceta, Avery August, Michihiro Hide, and Balázs István Tóth for their contribution to the peer review of this work. A peer review file is available.

a

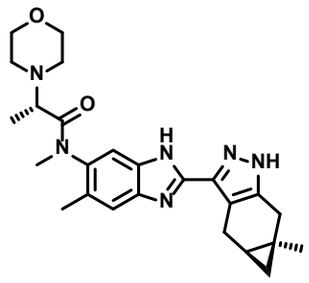

PF-07245303

b

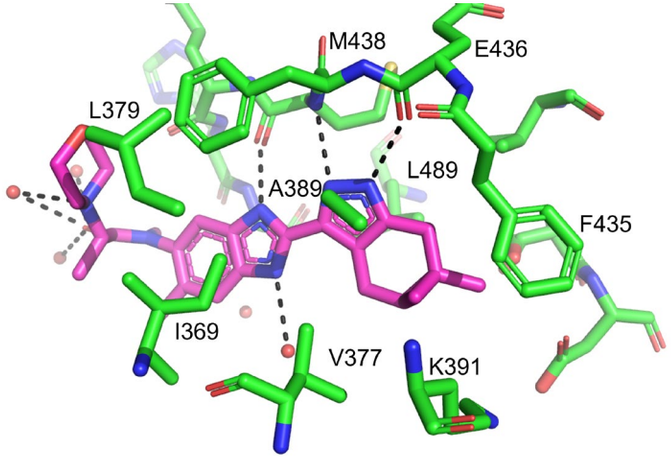

c

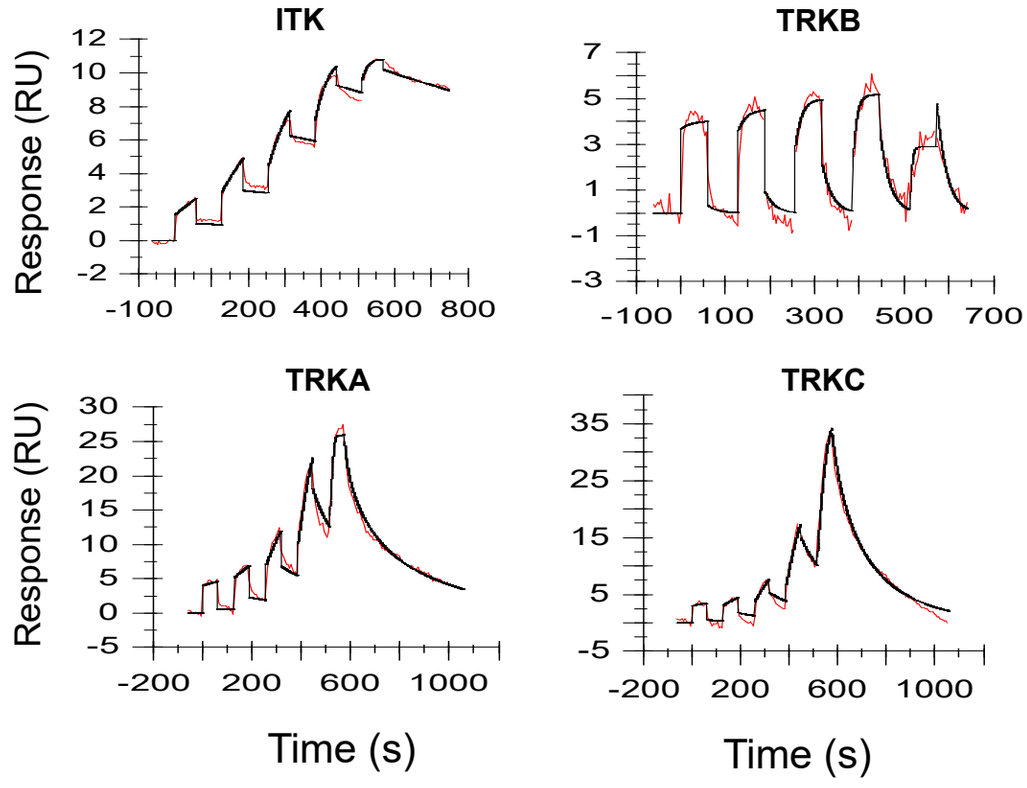

d

Phys. prop	Value
MW	**449**
SFLogD	**3.4**
MDCK-LE (10^{-6} cm/sec)	**13**
HLM (Clia µL/min/mg protein)	**188**
hHEP (Clia µL/min/million cells)	**30**
human PPB Fu	**0.11**
human BPR	**1.26**
Thermodynamic Solubility pH 7.4 (µM)	**40.5**

e

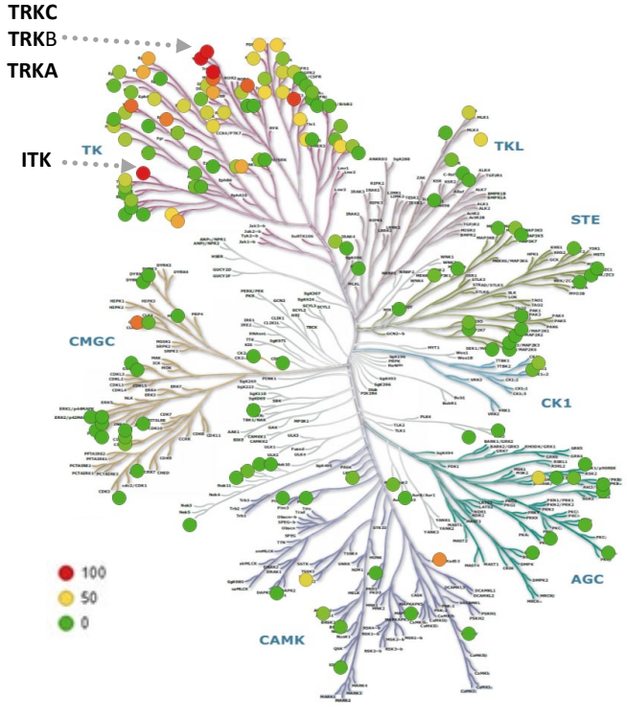

Immobilized Ligand	n	ka (1/Ms)	kd (1/s)	K_D (nM)	$T_{1/2}$ (minutes)
ITK	11	1.46E+06 ± 6.73E+05	9.94E-04 ± 4.69E-04	0.71 ± 0.22	13.8 ± 5
TRKA	6	9.76E+06 ± 2.65E+06	2.92E-02 ± 1.07E-02	2.94 ± 0.54	0.46 ± 0.2
TRKB	6	4.14E+06 ± 2.43E+06	2.78E-02 ± 1.40E-02	8.73 ± 6.2	0.53 ± 0.3
TRKC	6	4.28E+06 ± 4.75E+06	3.11E-02 ± 2.58E-02	10.0 ± 5.2	0.75 ± 0.7

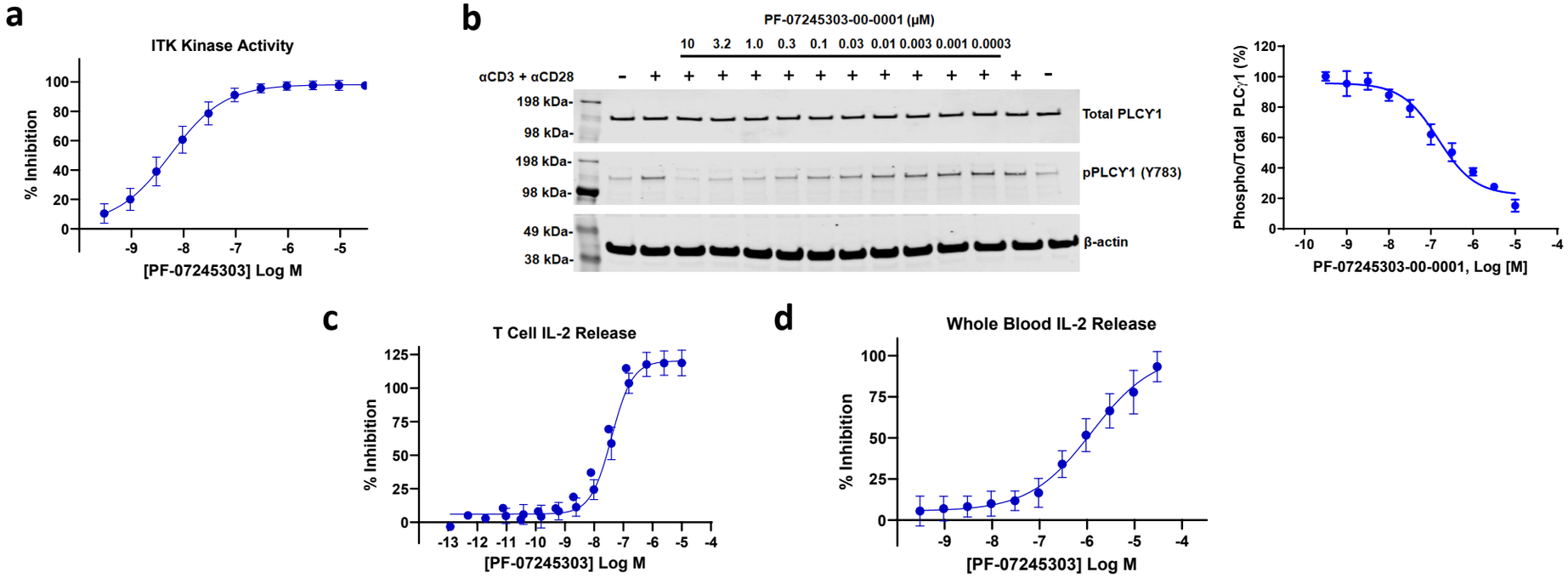
a
ITK Kinase Activity
% Inhibition
[PF-07245303] Log M
b
PF-07245303-00-0001 (μM)
10 3.2 1.0 0.3 0.1 0.03 0.01 0.003 0.001 0.0003
αCD3 + αCD28
198 kDa-
98 kDa-
Total PLCY1
pPLCY1 (Y783)
49 kDa-
38 kDa-
β-actin
Phospho/Total PLCγ1 (%)
PF-07245303-00-0001, Log [M]
c
T Cell IL-2 Release
% Inhibition
[PF-07245303] Log M
d
Whole Blood IL-2 Release
% Inhibition
[PF-07245303] Log M

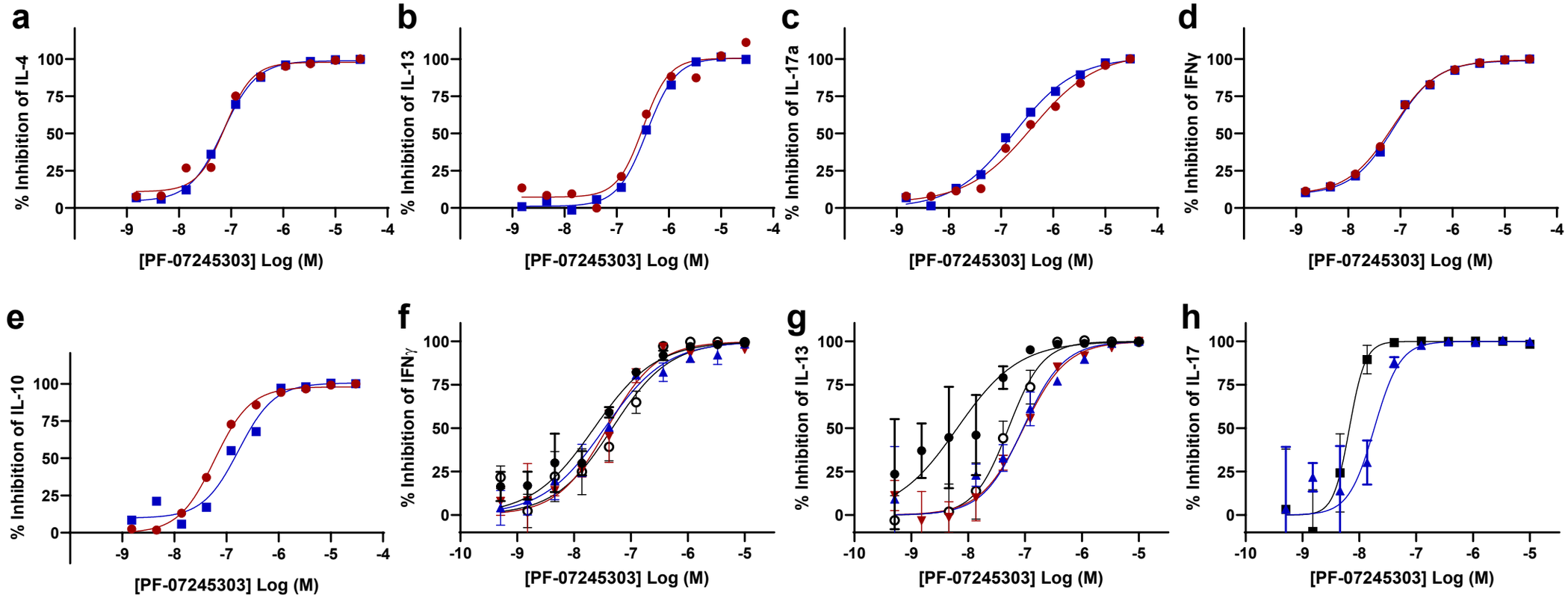
a
% Inhibition of IL-4
[PF-07245303] Log (M)
b
% Inhibition of IL-13
[PF-07245303] Log (M)
c
% Inhibition of IL-17a
[PF-07245303] Log (M)
d
% Inhibition of IFNγ
[PF-07245303] Log (M)
e
% Inhibition of IL-10
[PF-07245303] Log (M)
f
% Inhibition of IFNγ
[PF-07245303] Log (M)
g
% Inhibition of IL-13
[PF-07245303] Log (M)
h
% Inhibition of IL-17
[PF-07245303] Log (M)

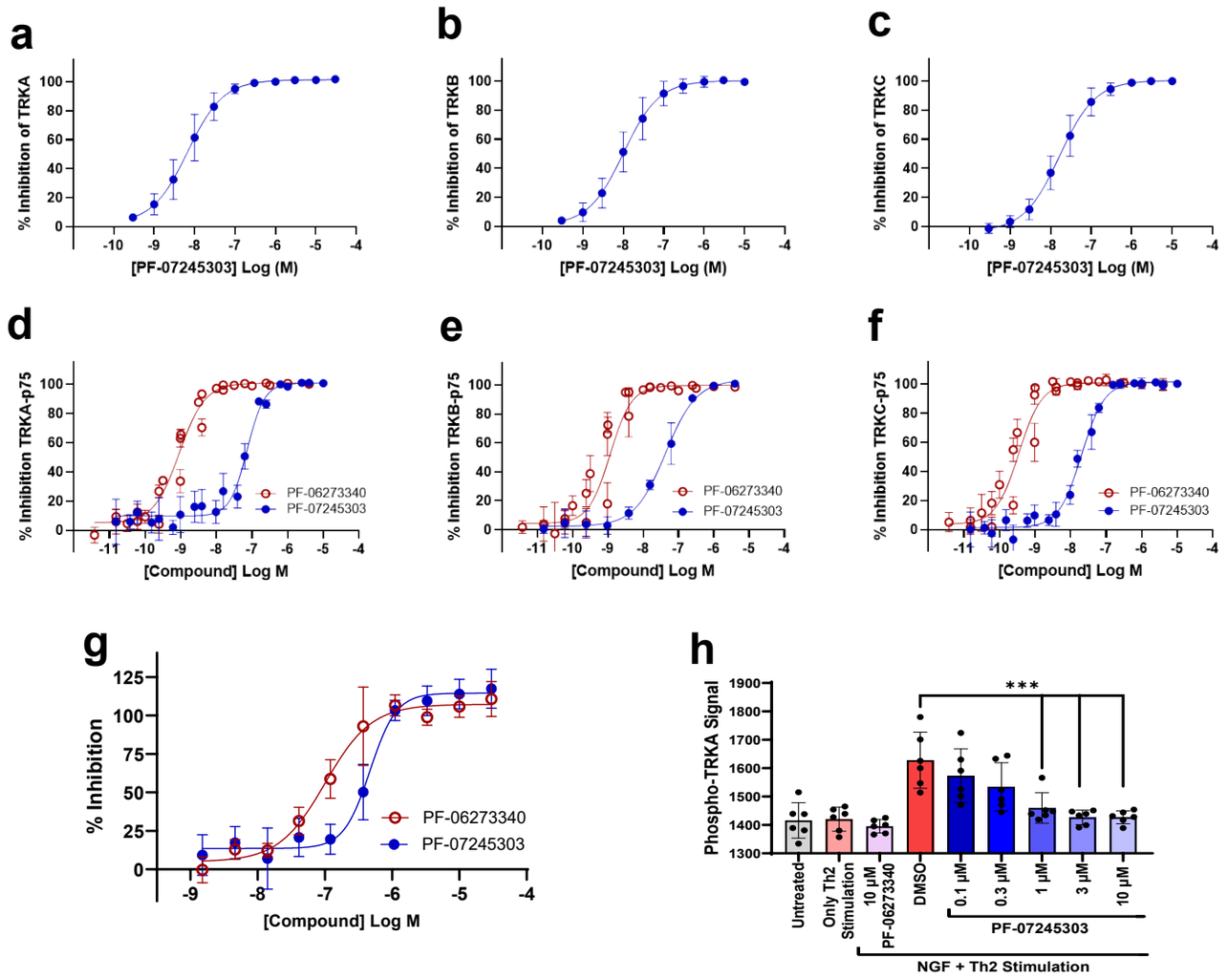
a
% Inhibition of TRKA
[PF-07245303] Log (M)
b
% Inhibition of TRKB
[PF-07245303] Log (M)
c
% Inhibition of TRKC
[PF-07245303] Log (M)
d
% Inhibition TRKA-p75
[Compound] Log M
PF-06273340
PF-07245303
e
% Inhibition TRKB-p75
[Compound] Log M
PF-06273340
PF-07245303
f
% Inhibition TRKC-p75
[Compound] Log M
PF-06273340
PF-07245303
g
% Inhibition
[Compound] Log M
PF-06273340
PF-07245303
h
Phospho-TRKA Signal
***
Untreated
Only Th2 Stimulation
10 µM PF-06273340
DMSO
0.1 µM
0.3 µM
1 µM
3 µM
10 µM
PF-07245303
NGF + Th2 Stimulation

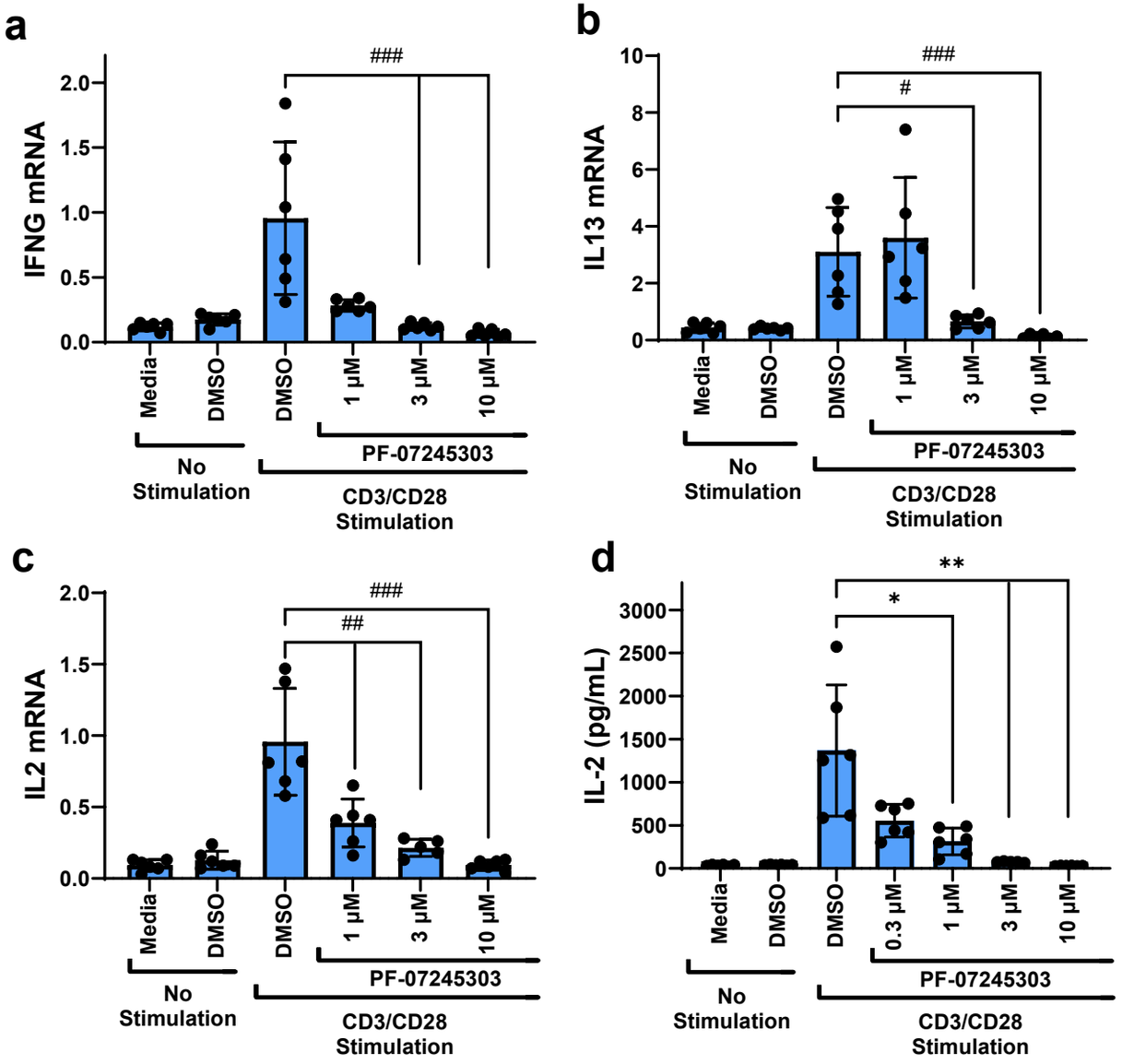
a
IFNG mRNA
2.0
1.5
1.0
0.5
0.0
###
Media
DMSO
DMSO
1 µM
3 µM
10 µM
No Stimulation
PF-07245303
CD3/CD28 Stimulation
b
IL13 mRNA
10
8
6
4
2
0
###
#
Media
DMSO
DMSO
1 µM
3 µM
10 µM
No Stimulation
PF-07245303
CD3/CD28 Stimulation
c
IL2 mRNA
2.0
1.5
1.0
0.5
0.0
###
##
Media
DMSO
DMSO
1 µM
3 µM
10 µM
No Stimulation
PF-07245303
CD3/CD28 Stimulation
d
IL-2 (pg/mL)
3000
2500
2000
1500
1000
500
0
**
*
Media
DMSO
DMSO
0.3 µM
1 µM
3 µM
10 µM
No Stimulation
PF-07245303
CD3/CD28 Stimulation

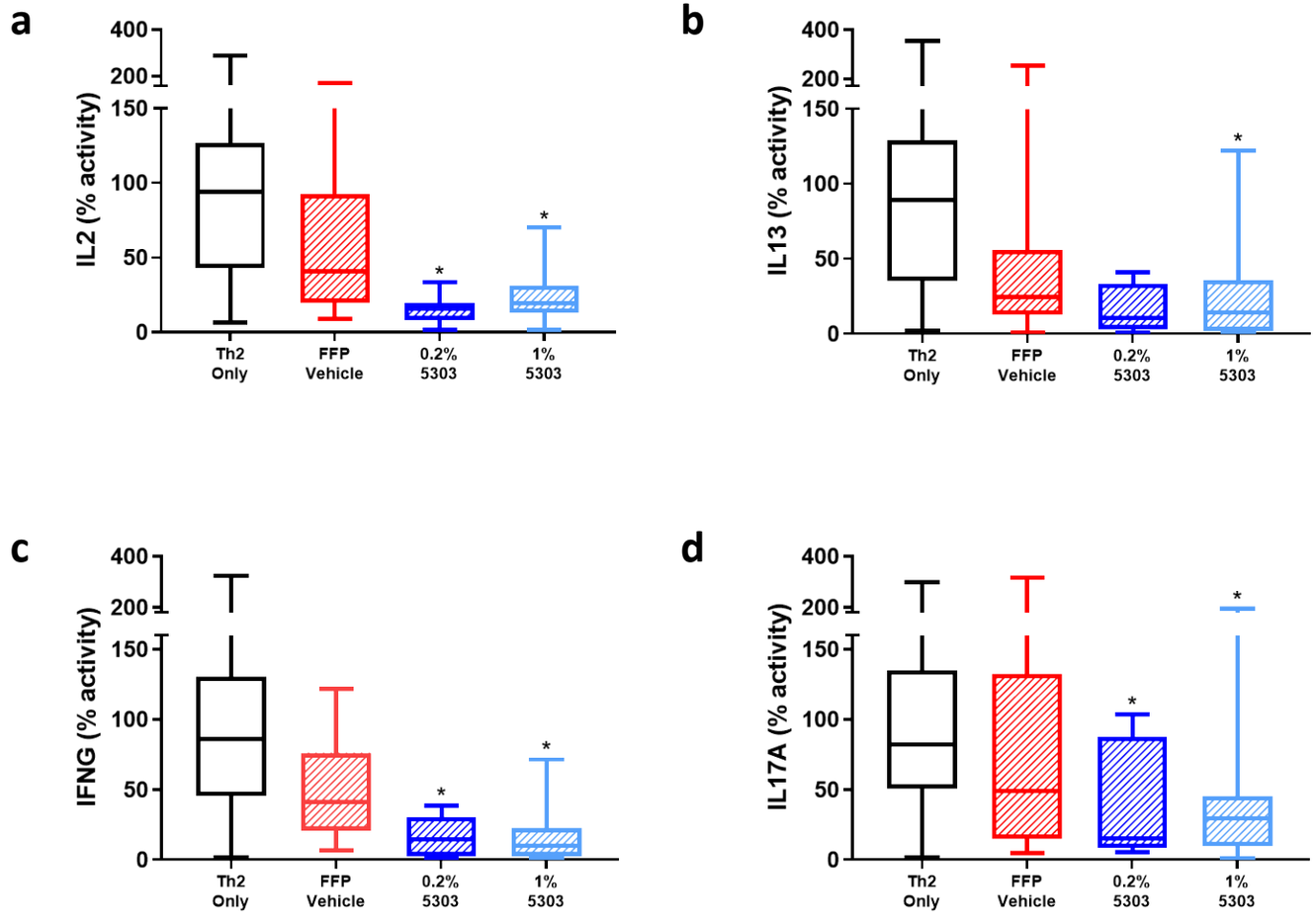
a
IL2 (% activity)
400
200
150
100
50
0
*
*
Th2 Only
FFP Vehicle
0.2% 5303
1% 5303
b
IL13 (% activity)
400
200
150
100
50
0
*
Th2 Only
FFP Vehicle
0.2% 5303
1% 5303
c
IFNG (% activity)
400
200
150
100
50
0
*
*
Th2 Only
FFP Vehicle
0.2% 5303
1% 5303
d
IL17A (% activity)
400
200
150
100
50
0
*
*
Th2 Only
FFP Vehicle
0.2% 5303
1% 5303

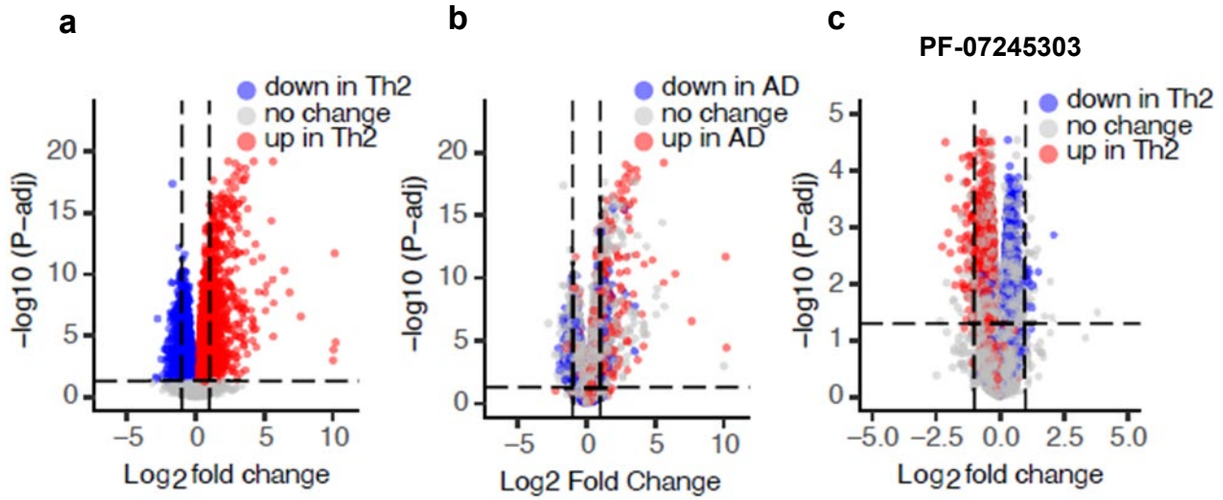
a
down in Th2
no change
up in Th2
−log10 (P−adj)
Log2 fold change
b
down in AD
no change
up in AD
−log10 (P−adj)
Log2 Fold Change
c
PF-07245303
down in Th2
no change
up in Th2
−log10 (P−adj)
Log2 fold change

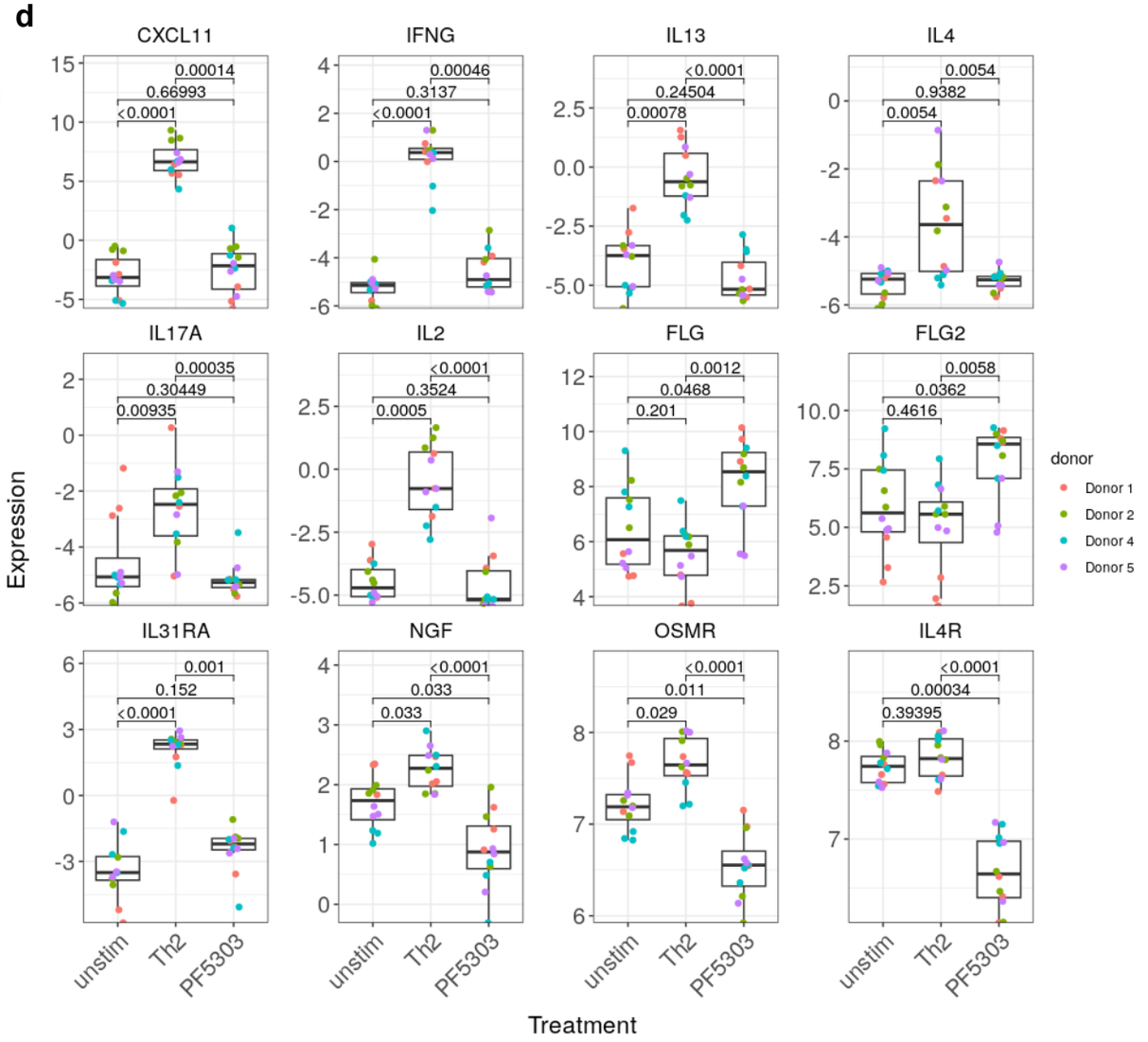
d
CXCL11
IFNG
IL13
IL4
IL17A
IL2
FLG
FLG2
IL31RA
NGF
OSMR
IL4R
Expression
unstim
Th2
PF5303
Treatment
donor
Donor 1
Donor 2
Donor 4
Donor 5

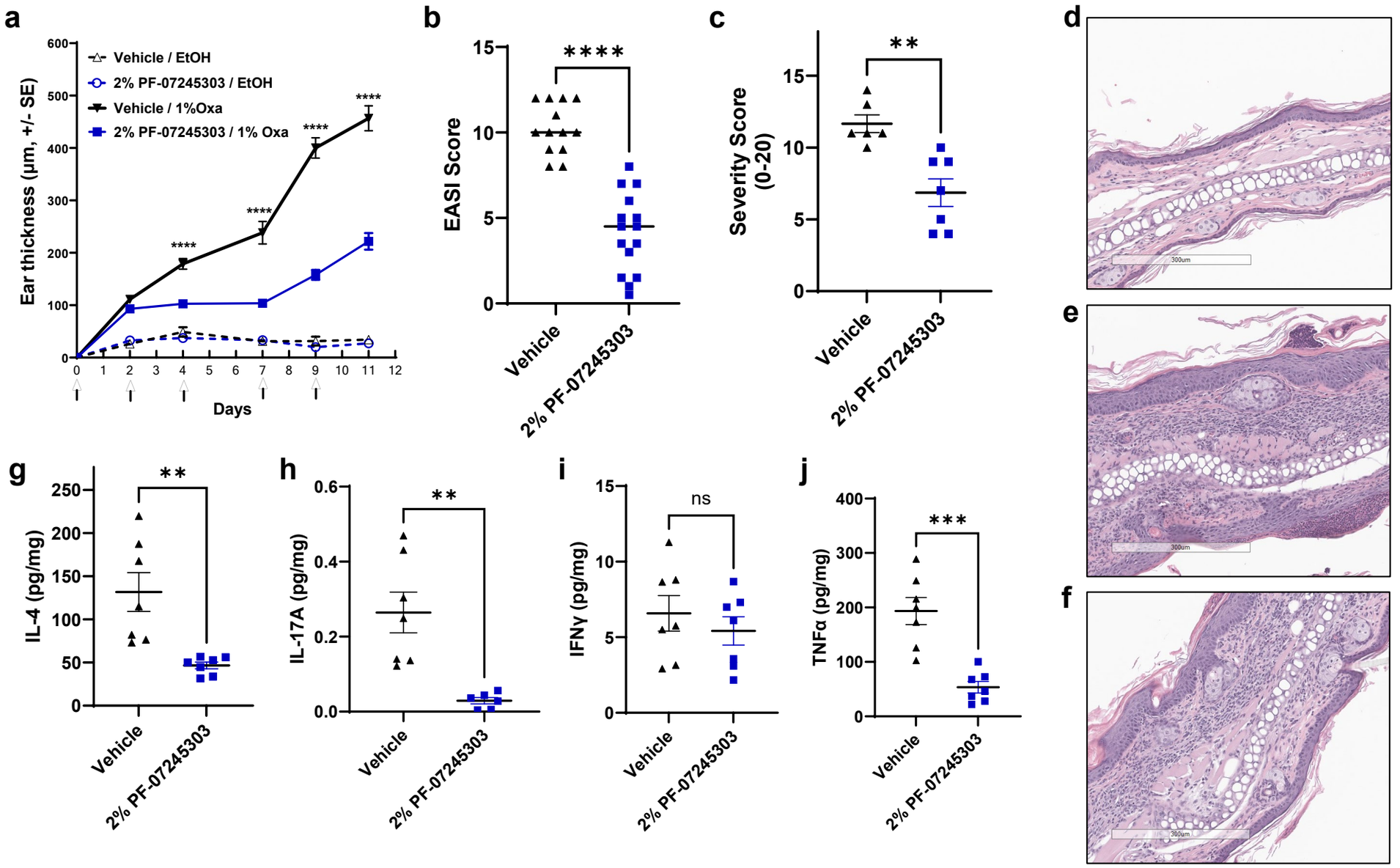
a
Vehicle / EtOH
2% PF-07245303 / EtOH
Vehicle / 1%Oxa
2% PF-07245303 / 1% Oxa
Ear thickness (µm, +/- SE)
Days
****
b
EASI Score
****
Vehicle
2% PF-07245303
c
Severity Score (0-20)
**
Vehicle
2% PF-07245303
d
e
f
g
IL-4 (pg/mg)
**
h
IL-17A (pg/mg)
**
i
IFNγ (pg/mg)
ns
j
TNFα (pg/mg)
***